RESEARCH ARTICLE



Check for updates

WILEY

Tracer-aided ecohydrological modelling across climate, land cover, and topographical gradients in the tropics

Saul Arciniega-Esparza^{1,2} | Christian Birkel^{1,3,4} | Ana María Durán-Quesada^{5,6} | Ricardo Sánchez-Murillo⁷ | Georgianne W. Moore⁸ | Marco P. Maneta⁹ | Jan Boll¹⁰ | Laura Benegas Negri⁴ | Dörthe Tetzlaff^{11,12} | Kei Yoshimura¹³ | Chris Soulsby³ |

Correspondence

Saul Arciniega-Esparza, Department of Geography and Water and Global Change Observatory, University of Costa Rica, San José, Costa Rica.

Email: sarciniegae@comunidad.unam.mx

Funding information Leverhulme Trust

Abstract

Quantitative estimations of ecohydrological water partitioning into evaporation and transpiration remains mostly based on plot-scale investigations that use well-instrumented, small-scale experimental catchments in temperate regions. Here, we attempted to upscale and adapt the conceptual tracer-aided ecohydrology model STARRtropics to simulate water partitioning, tracer, and storage dynamics over daily time steps and a 1-km grid larger-scale (2565 km²) in a sparsely instrumented tropical catchment in Costa Rica. The model was driven by bias-corrected regional climate model outputs and was simultaneously calibrated against daily discharge observations from 2 to 30 years at four discharge gauging stations and a 1-year, monthly streamwater isotope record of 46 streams. The overall model performance for the best discharge simulations ranged in KGE values from 0.4 to 0.6 and correlation coefficients for streamflow isotopes from 0.3 to 0.45. More importantly, independent model-derived transpiration estimates, point-scale residence time estimates, and measured groundwater isotopes showed reasonable model performance and simulated spatial

This is an open access article under the terms of the Creative Commons Attribution-NonCommercial License, which permits use, distribution and reproduction in any medium, provided the original work is properly cited and is not used for commercial purposes.

© 2023 The Authors. *Hydrological Processes* published by John Wiley & Sons Ltd.

¹Department of Geography and Water and Global Change Observatory, University of Costa Rica, San José, Costa Rica

²Hydrogeology Group, Faculty of Engineering, Universidad Nacional Autónoma de México, Mexico City, Mexico

³Northern Rivers Institute, University of Aberdeen, Aberdeen, UK

⁴Centro Agronómico Tropical de Investigación y Enseñanza (CATIE), Turrialba, Costa Rica

⁵Centro de Investigaciones Geofísicas, CIGEFI, Universidad de Costa Rica, San José, Costa Rica

⁶Centro de Investigación en Contaminación Ambiental, CICA, Universidad de Costa Rica, San José, Costa Rica

⁷Department of Earth and Environmental Sciences, University of Texas at Arlington, Arlington, Texas, USA

⁸Department of Biology, Georgia Southern University, Statesboro, Georgia, USA

⁹Department of Geosciences, University of Montana, Missoula, Montana, USA

¹⁰Civil and Environmental Engineering, Washington State University, Pullman, Washington, USA

¹¹Leibnitz-Institut für Gewasserökologie und Binnenfischerei (IGB), Berlin, Germany

¹²Humboldt Universitaet zu Berlin, Berlin, Germany

¹³University of Tokyo, Tokyo, Japan

KEYWORDS

Costa Rica, ecohydrology, stable isotopes, tracer-aided model, tropics, water partitioning

INTRODUCTION

Despite their importance, climate variability and change impacts on ecohydrological partitioning and water availability are still poorly understood in many global regions, particularly in tropical Costa Rica and Central America. This significant knowledge gap needs urgent attention, as extensive areas in Central America are, in addition to climate change (González et al., 2017), undergoing rapid land use conversion from pastures to crops (e.g., pineapple monocultures) and largescale reforestation initiatives (Min-Venditti et al., 2017). As vegetationmediated transpiration is the largest water flux to the atmosphere (e.g., Jasechko et al., 2013; Wei et al., 2016), large-scale land use transformations are likely to affect local to regional climate characteristics, water availability, sediment and nutrient dynamics, runoff generation and biodiversity assemblages (Lawrence & Vandecar, 2014).

Central America is a highly sensitive and vulnerable region in the world climate system (Giorgi, 2006), as the pulse of El Niño Southern Oscillation (ENSO) cycles is evident in sea surface temperature (SST) anomalies in the eastern Pacific as well as possible synchronized and counteractive temperature fluctuations in the Caribbean Sea. Both water bodies significantly influence climatic variability in Central America, affecting temperatures and rainfall as well as occurrence and intensity of extreme events such as droughts and heavy rainfall (Durán-Quesada et al., 2017). For example, Muñoz-Jiménez et al. (2019) showed that marked SST variations could simultaneously cause drought and flood events for Central America Pacific and Caribbean slopes, respectively, as evidence has shown during strong El Niño events (Hastenrath & Polzin, 2013; Pascale et al., 2021). Moreover, cyclone activity can be pronounced and contribute large volumes of rainfall to the region causing large-scale flooding and landslides (Sánchez-Murillo et al., 2019). Tropical cyclones, and other tropical disturbances such as easterly waves and cyclones, not only produce extreme ranges of rainfall volumes but also immense stable isotope variability in the precipitation input signal (Welsh & Sánchez-Murillo, 2020). As a result, Costa Rica is characterized by high spatial heterogeneity and temporal variability in hydroclimate and is vulnerable to extreme climate change impacts (Durán-Quesada et al., 2020). Furthermore, Costa Rica is also characterized by relative data scarcity like most tropical countries (Wohl et al., 2012), which was locally exacerbated due to recent impacts by, for example, the COVID-19 pandemic.

Implications for water availability are intimately connected to ecohydrological partitioning under contrasting land use types and how much water is intercepted, evaporated, transpired, or recharged into aquifers for streamflow generation across contrasting spatial and temporal scales. It is still challenging to measure most ecohydrological partitioning directly, and field measurements are almost exclusively restricted to plot-scale studies (Beyer et al., 2020; Landgraf et al., 2022). Direct measurements include Eddy Covariance and sap flux-derived transpiration rates, such as in Aparecido et al. (2016) for a pre-montane rainforest in Costa Rica or stable isotope-based tracer methods (Xiao et al., 2018). In-situ stable isotope measurements to understand water partitioning are still rare particularly for the tropics (pioneering work by Moreira et al., 1997), and Kühnhammer et al. (2022) presented one recent example for the tropics. Additionally, it is notoriously difficult to extrapolate results to catchment scales (Moore et al., 2018) which are more relevant to water and risk management decision making.

Recent experimental and modelling work has shown that environmental tracers, particularly stable water isotopes, can be used as an ARCINIEGA-ESPARZA ET AL. WII FY 3 of 20

additional source of information (within models or alone) that can integrate insights into water sources, flow paths, mixing processes, and associated travel times across scales (see Birkel & Soulsby, 2015 for a review). Tracer insights can be invaluable for more quantitative estimates of hydrological processes and ecohydrological partitioning even at catchment scales (Knighton et al., 2017; Rodriguez & Klaus, 2019). For example, Iraheta et al. (2021) covered the territory of Costa Rica using a simple isotope mass balance to estimate ecohydrological water partitioning.

Therefore, models as simulation tools are still the most widely applied technique for upscaling and estimating ecohydrological water partitioning over larger areas. Recent research has shown that the direct tracking of stable isotopes in such models provides important additional information to increase confidence in model evaluation and hypothesis testing (see Correa et al. (2020) and Remondi et al. (2018) for a conceptual approach, Kuppel et al. (2018) and Smith et al. (2021) for a physically based approach to tracer-aided ecohydrological modelling). Such tracer-aided models (TAMs) have been shown to help reduce parameter uncertainty and provide water flux and storage estimates that align with independent measurements such as soil moisture and groundwater levels (Birkel et al., 2014). Building on previous small-scale (3.2 km²) experimental studies with the TAM "STARRtropics" (Correa et al., 2020), here we attempted to upscale (2565 km²) the ecohydrology model for water partitioning, tracer and storage dynamics, leveraging a unique monthly stable isotope data set of 46 sampled rivers (Birkel et al., 2020) in the San Carlos study catchment in Costa Rica. We hypothesized that land cover dominates over topography in shaping transpiration patterns and ecohydrological partitioning and asked the following research questions:

- 1. Are the catchment-scale hydrological processes represented in the STARRtropics model capable of capturing the diversity of streamflow responses in a 2565 km² tropical catchment?
- 2. What is the information content found in distributed stream and groundwater isotope measurements for regional rainfall-runoff, storage and ecohydrological water partitioning simulations in an heterogenous tropical landscape?
- 3. How limiting is the isotopic rainfall reanalysis model input for capturing ecohydrological dynamics in a distributed, tracer-aided model?

2 | STUDY CATCHMENT

The San Carlos River catchment (2565 km²) in northeastern Costa Rica drains into the San Juan River at the Nicaraguan border (Figure 1) and represents a large-scale catchment in the context of Central America (Gleeson & Paszkowski, 2014). The complex, nested catchment system has an area of around 2413 km² at the downstream gauging station Boca Tapada at 10 km to the confluence (station 41 in Figure 1d). The system drains from the Central Volcanic Cordillera at the continental divide at a maximum elevation of 2326 m.a.s.l. (active Platanar volcano to the southeast) down into the

Caribbean plains at around 30 m.a.s.l. (Figure 1a,d). Two active volcanoes (Arenal and Platanar) in the catchment are the source of young basaltic and andesitic rocks dating from the Holocene. Downstream of the active volcanoes, the age of the rocks increases up to $5-9\ \text{Mio}$ years (Miocene). More recent Late Quaternary fluvial and marine deposits dominate the lowlands but eroded volcanic remnants along major fault lines can still be detected in the field. The geology results in mostly volcanic soils differentiated according to their development stage, with less developed Entisols to deeper Andisols in the headwaters and older Ultisols in the mid and lowlands. The steep uplands with high hydraulic gradients, high material transport capacity, and dynamic streamflow regimes correspond to almost completely protected rainforests and cloud forests under the National Park system (plus some private reserves) that transition at lower elevations below 1500 m.a.s.l. into a pasture and grazing system (Figure 1b). The lowlands below 200 m.a.s.l. are dominated by extensive, and in parts industrial, agriculture (e.g., pineapple and sugarcane). Lowland rainforests remain only close to the catchment outlet.

The climate is influenced by the Caribbean Low-Level Jet (CLLJ; Amador, 2008) and the Inter Tropical Convergence Zone (ITCZ), with moisture supply from the Caribbean contributing to precipitation and high relative humidity throughout the year (Durán-Quesada et al., 2017). Mean annual catchment precipitation (MAP) of around 4000 mm, and the spatial variability from 3000 to 5500 mm, are caused by the varied topography (Figure 1e). Close to the continental divide, the Pacific climate domain, with a marked dry season from December to April and rainfall events mainly between May and November (Solano-Rivera et al., 2019), are characterized as an intraannual rainfall regime (Taylor et al., 2002). Air temperature closely follows the environmental lapse rate (-6° C/1000 m) with on average 26°C in the lowlands and below 20°C at elevations above 1000 m.a. s.l.

3 | DATA AND METHODS

3.1 Data sources and corrections

3.1.1 | Meteorological data, catchment properties, and model input

Model input used a catchment land cover classification (Figure 1b), the Topographical Wetness Index (TWI, Figure 1c), and the Leaf Area Index (LAI, Figure 1d). The TWI was derived from a national 10-m digital elevation model (Table 1). Land cover was classified using a recent cloud-free Sentinel 2 satellite imagery mosaic and verified in the field (Figure 1b). The temporally averaged, but spatially-distributed LAI map was calculated from the mean monthly aggregation of MODIS satellite product MOD15A2 from 2000 to 2018 (Myneni et al., 2015; Tian et al., 2002). Mean monthly catchment MODIS LAI values oscillate between 1.5 (lowest LAI in July) and 3.5 (maximum LAI in February) in comparison to an overall catchment mean of 2.4 derived from Figure 1d used for modelling. We used simulated temperature,

10991085, 2023, 5, Downloaded from https://onlinelbitary.wiley.com/doi/10.1002/hpp.14884, Wiley Online Library on [0.1052023]. See the Terms and Conditions (https://onlinelbitary.wiley.com/terms-and-conditions) on Wiley Online Library for rules of use; OA articles are governed by the applicable Creative Commons Licenses

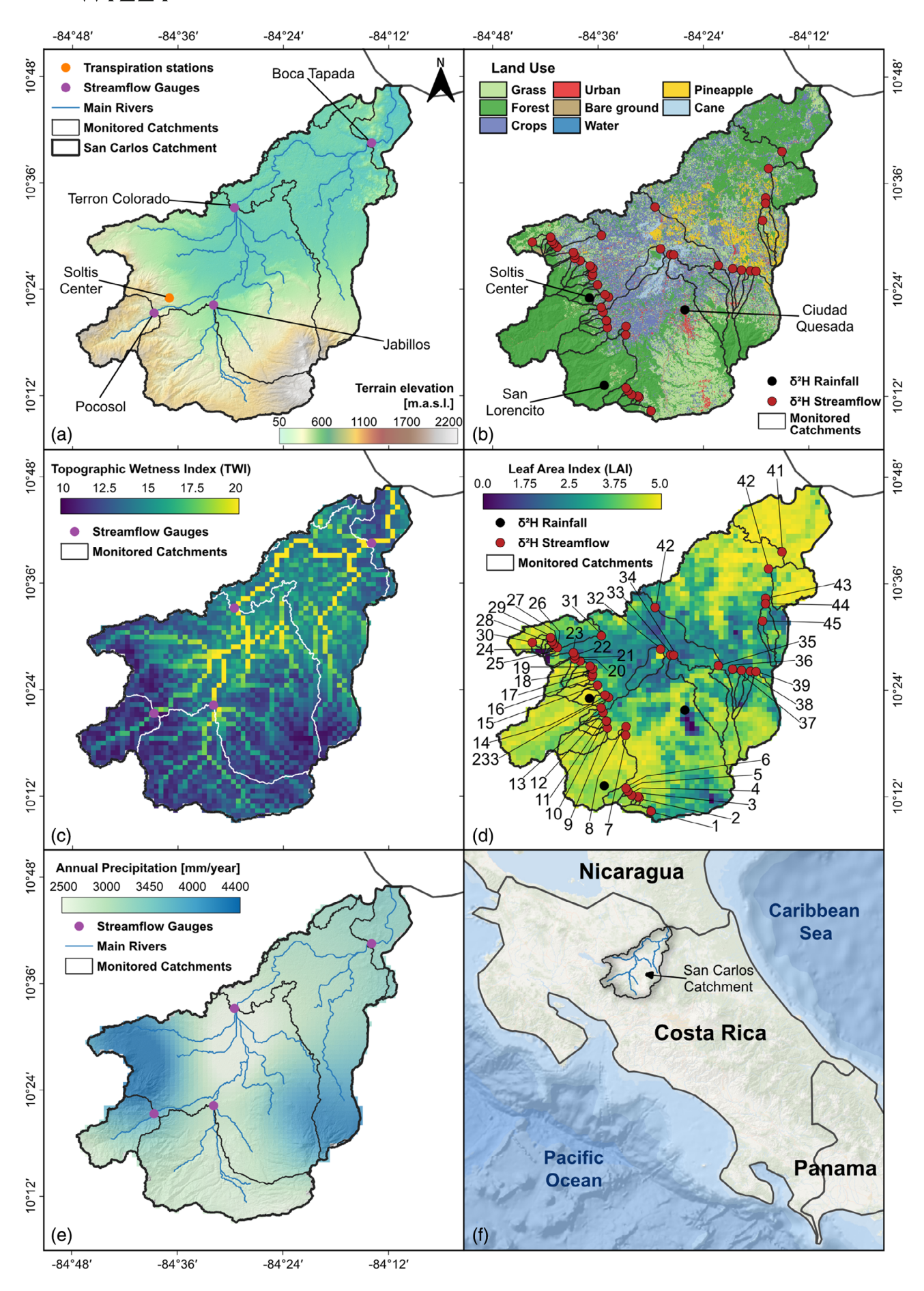


FIGURE 1 Legend on next page.

relative humidity, and isotopic composition of precipitation from outputs of the isotope-enabled regional climate model IsoRSM (Yoshimura et al., 2010) to drive our ecohydrology model STARRtropics from 1983 to 2018 (Figure 2). The IsoRSM simulations were performed over Central America (pers. Comm. Ana María Duran-Quesada) with a horizontal resolution of 10 km and 15 vertical layers at hourly temporal resolution. Lateral conditions for the regional simulations were obtained from global simulations with IsoGSM (Yoshimura et al., 2008), which resulted in good correlations of simulated and observed rainfall rate (Tropical Rainfall Measurement Mission, TRMM) of 0.88 and total precipitable water (r = 0.72) for Central America, albeit a larger bias was identified over mountain areas and the Caribbean coast. The validation of the isotopic composition of rainfall was based on limited available records mostly from the Pacific slope of Costa Rica, but IsoRSM showed good skill (r > 0.5) using a point to pixel comparison.

Daily precipitation from the bias-corrected global product CHIRPSv2 (Funk et al., 2015) generated by Arciniega-Esparza et al. (2022) for Costa Rica was used as forcing, which was checked against the Soltis Center station data (Figure 1a) with a good agreement $(R^2 > 0.8)$. This already corrected precipitation product matches the overall water balance of the San Carlos and closely agrees with the rainfall regimes of the modelled IsoRSM precipitation output but was preferred due to the higher spatial resolution of CHIRPS (\sim 5 × 5 km vs. \sim 10 \times 10 km) to capture the topographical precipitation gradient and the observed daily rainfall-runoff response. Matching rainfall regimes of both the corrected CHIRPS and IsoRSM product allowed transfer of precipitation isotope composition for ecohydrology modelling. Transpiration at the Soltis Center for Research and Education of Texas A&M University (Figure 1a) was estimated based on sap flow measurements (Aparecido et al., 2016) and used for independent model evaluation.

3.1.2 | Hydrological data

Discharge records are sparse in the catchment, and we used publicly available data for four discharge gauging stations (from the Costa Rican Electricity Institute ICE hydrology bulletins; ICE, n.d.) for model calibration; covering spatial scales from around 100 km² to the lowest monitored site at 2413 km² (Boca Tapada station). For the smallest gauged 3.2 km² catchment (RBAMB) we used more recent discharge data from 2015 to 2018 only for independent model evaluation (Figure 1a). Table 1 shows the discharge stations with associated catchment properties and discharge statistics. Only the Terron

Colorado station has a long-term record with data from 1973 to 2003. The discharge records from the Boca Tapada, Jabillos, and Pocosol stations are available only from 1988 to 1990.

3.1.3 | Tracer (stable isotope) data

We sampled 46 accessible rivers across the entire catchment monthly for isotope analysis from June 2018 until May 2019 covering upland streams to the downstream San Carlos River (Figure 1b and Table 1). The catchments were selected to cover all gauged sites and to represent most of the nested sub-catchments (the complete data set from Birkel et al. (2020) can be freely accessed at http://www.hydroshare.org/resource/e6b38a2999 354626a36058676f916a47). The monitored catchments ranged from 1 to 2412 km² with a mean area of 125 km² (standard deviation of 425 km²) and captured the whole elevation gradient with a mean catchment altitude of 619 m. The San Lorencito experimental headwater catchment isotope data from 2013 to 2019 were used for independent model evaluation. The sampled sub-catchments comprise the complete climatic, geologic, and land use gradient of the San Carlos River. Stable isotope analysis was performed in the laboratory of the Stable Isotopes Research Group, Universidad Nacional (UNA-SIL, Costa Rica). All samples were collected in 30 mL HDPE bottles with plastic inserts to prevent secondary evaporation. Samples were filtered using a Midisart PTFE (polytetrafluorethylene) 0.45 mm syringe membrane (Sartorius AG, Germany) and stored at 5°C until analysis. Isotope measurements were conducted within 3-5 days after sampling. The streamwater samples were analysed for deuterium (δ^2 H) and oxygen-18 (δ^{18} O) using an LWIA-45-EP water isotope analyser (Los Gatos, USA). The average sample analytic precision during the analysis was 0.06% for δ^{18} O and 0.33% for δ^{2} H. The average analytic precision for the enriched $(\delta^{18}O = -2.24\%, \ \delta^2H = -10.30\%)$ and depleted $(\delta^{18}O = -16.73\%, \ \delta^2H = -10.30\%)$ $\delta^2 H = -130.28\%$) standards were 0.07% for $\delta^{18} O$ and 0.28% for $\delta^2 H$ and 0.07% for δ^{18} O and 0.38% for δ^{2} H, respectively. The isotope ratios are presented in the established delta notation δ (%), with reference to the VSMOW-SLAP scale. Precipitation at the Soltis Center for Research and Education of Texas A&M University (Figure 1a) was collected daily at 6 AM, sealed in the same HDPE bottles, and stored in a fridge at 4°C until shipped to UNA-SIL for stable isotope analysis. Historic weekly (Cuidad Quesada) and event (San Lorencito) precipitation isotope records (Figure 1a) were also used for a linear scaling bias correction (see Wörner et al., 2019) of IsoRSM output (Figure 3) driving STARRtropics. The biascorrected precipitation isotope records capture the general variations but not the daily extremes (Figure 3). Still, the spatially variable precipitation isotope input is a useful basis for assessing more seasonal and interannual variations of system function in terms of flux and storage dynamics.

TABLE 1 Catchment discharge gauging station and isotope statistics used for model calibration, which are linked to the catchment map in Figure 1 for isotope sampling and gauging stations.

Catchments							Discharge statistics (m ³ /s)			
Upslope	Name		Area (km²)	Elevation (ı	m.a.s.l.)	Slope (%)	25%	50%		75%
Total	San Ca	rlos	2564.5	488		17.9				
Discharge gauges	Terron	Colorado	1699.3	647		21.2	78.30	137.00		197.00
	Boca T	apada	2412.6	336		13.5	97.80	179.00		278.75
	Jabillos	i	457.1	1005		29.7	19.50	35.80		64.02
	Pocoso	d	142.2	1170		41.0	10.80	16.40		22.17
Upslope	Name	Area (km²)	Elevation ((m.a.s.l.)	Slope (%)	δ ² H (‰)	δ ¹⁸ Ο	(‰)	San	ple size
Sampling points	1	7.9	1212	-	18.1	-32.8 ± 7.3	-5.62	2 ± 1.20	12	
	2	1.1	1108	3	18.7	-35.7 ± 3.2	-6.06	5 ± 0.48	12	
	3	1.6	1093	-	19.1	-37.6 ± 3.1	-6.32	2 ± 0.43	12	
	4	5.7	1158	3	31.0	-34.7 ± 3.2	-6.03	3 ± 0.54	12	
	5	1.0	1024	2	25.9	-32.9 ± 4.4	-5.75	5 ± 0.69	12	
	6	10.4	1098	3	37.5	-31.6 ± 2.9	-5.64	± 0.57	12	
	7	153.3	913	(35.2	-28.9 ± 4.4	-5.18	3 ± 0.73	11	
	8	1.5	271	-	18.0	-29.1 ± 5.4	-4.93	3 ± 0.84	12	
	9	38.2	964	4	42.0	-26.4 ± 4.1	-4.92	2 ± 0.68	12	
	10	7.2	767	(31.4	-25.7 ± 4.9	-4.71	± 0.78	12	
	11	5.7	571	2	24.0	-27.1 ± 3.9	-4.98	3 ± 0.66	12	
	12	5.8	664	;	30.3	-24.8 ± 8.1	-4.45	5 ± 1.25	12	
	13	152.8	1129	2	41.2	-24.4 ± 7.1	-4.68	3 ± 1.04	12	
	14	11.6	539	2	25.5	-25.9 ± 6.1	-4.83	3 ± 0.89	12	
	15	12.6	816	(38.6	-23.5 ± 7.7	-4.54	+ ± 1.15	12	
	16	8.4	628		34.6	-24.3 ± 8.6		3 ± 1.21	11	
	17	0.7	280	-	17.6	-26.9 ± 6.1	-4.72	2 ± 0.92	12	
	18	0.4	226		20.2	-26.3 ± 5.7		5 ± 0.86	11	
	19	7.1	364		24.2	-26.8 ± 7.0		L ± 1.02	10	
	20	7.4	609	(32.3	-23.0 ± 7.4	-4.51	L ± 1.02	11	
	21	22.6	853		33.7	-21.2 ± 6.3	-4.37	7 ± 0.90	12	
	22	1.6	537		21.2	-23.0 ± 8.3		5 ± 1.07	11	
	23	9.3	630		27.5	-23.9 ± 7.5		3 ± 0.92	12	
	24	0.8	625		30.6	-20.5 ± 3.2		± 0.57	12	
	25	0.5	517		24.7	-21.2 ± 1.3		9 ± 0.42	11	
	26	1.7	654		27.9	-20.8 ± 7.4) ± 1.20	10	
	27	0.5	525		21.5	-23.4 ± 2.8		3 ± 0.51	11	
	28	2.8	702		26.6	-21.4 ± 5.6		2 ± 0.85	10	
	29	4.4	540		15.6	-24.8 ± 10.2		5 ± 1.34	11	
	30	3.8	786		31.5	-21.1 ± 1.2		2 ± 0.36	11	
	31	95.9	450		17.7	-23.1 ± 2.7) ± 0.57	12	
	32	28.8	92		4.5	-27.3 ± 9.0		5 ± 1.23	12	
	33	778.9	874		25.1	-31.0 ± 3.9		5 ± 0.81	12	
	34	90.3	432		14.7	-27.1 ± 3.7		9 ± 0.63	12	
	35	44.9	1099	(36.9	-26.2 ± 3.6		9 ± 0.64	12	
	36	9.1	286		7.8	-27.5 ± 3.7		L ± 0.68	12	
	37	8.9	315		9.6	-26.8 ± 3.3		5 ± 0.61	12	
	38	11.9	363		9.9	-26.1 ± 3.7	-4.48	3 ± 0.65	12	

TABLE 1 (Continued)

Upslope	Name	Area (km²)	Elevation (m.a.s.l.)	Slope (%)	δ ² H (‰)	δ ¹⁸ O (‰)	Sample size
	39	99.4	684	24.0	-24.2 ± 3.3	-4.55 ± 0.53	12
	40	1591.4	683	22.2	-27.3 ± 4.8	-4.85 ± 0.77	10
	41	2370.1	113	7.1	-25.6 ± 6.6	-4.48 ± 1.01	10
	42	66.1	127	18.2	-19.9 ± 4.8	-3.62 ± 0.90	10
	43	30.0	119	6.7	-20.6 ± 4.2	-3.58 ± 0.86	10
	44	28.9	104	5.0	-21.3 ± 3.8	-3.67 ± 0.81	10
	45	9.4	130	5.1	-22.2 ± 2.8	-3.81 ± 0.67	10
	233	5.0	357	13.5	-26.3 ± 6.5	-4.46 ± 0.96	11

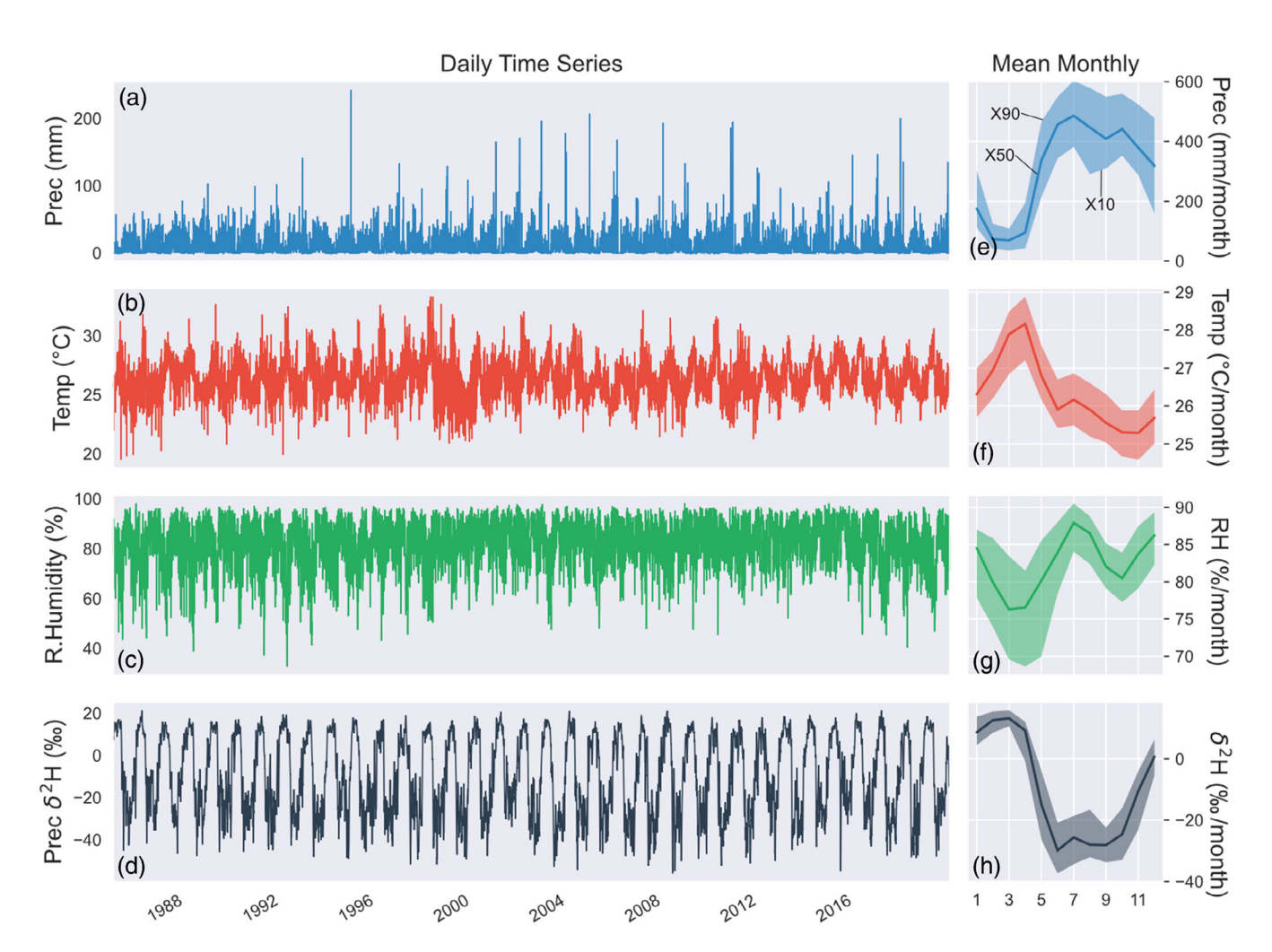


FIGURE 2 (a-d) Bias-corrected catchment average daily model forcing time series together with (e-h) mean monthly regimes of precipitation, temperature, relative humidity (RH), and precipitation isotopes (δ^2 H) for the study period from 1983 to 2018. The shaded bands around the monthly regimes are one standard deviation representing the overall variability. Note the inverse relationships of precipitation with precipitation isotopes and temperature with relative humidity.

3.2 Model setup and evaluation

The Spatially distributed, conceptual Tracer-Aided Rainfall-Runoff ecohydrology model for the tropics (STARRtropics), driven by biascorrected precipitation from CHIRPSv2 and IsoRSM output (Figure 4), was used in this study. This was based on previous small-scale (3.2 km²) and high-resolution (10 m grid and hourly time step) applications by Dehaspe et al. (2018) and Correa et al. (2020). The San Lorencito catchment test site is a headwater of the San Carlos River (Figure 1b). STARRtropics evolved from its initial development (as the model STARR) in northern upland catchments in Scotland (van Huijgevoort et al., 2016) to represent the pristine tropical rainforest

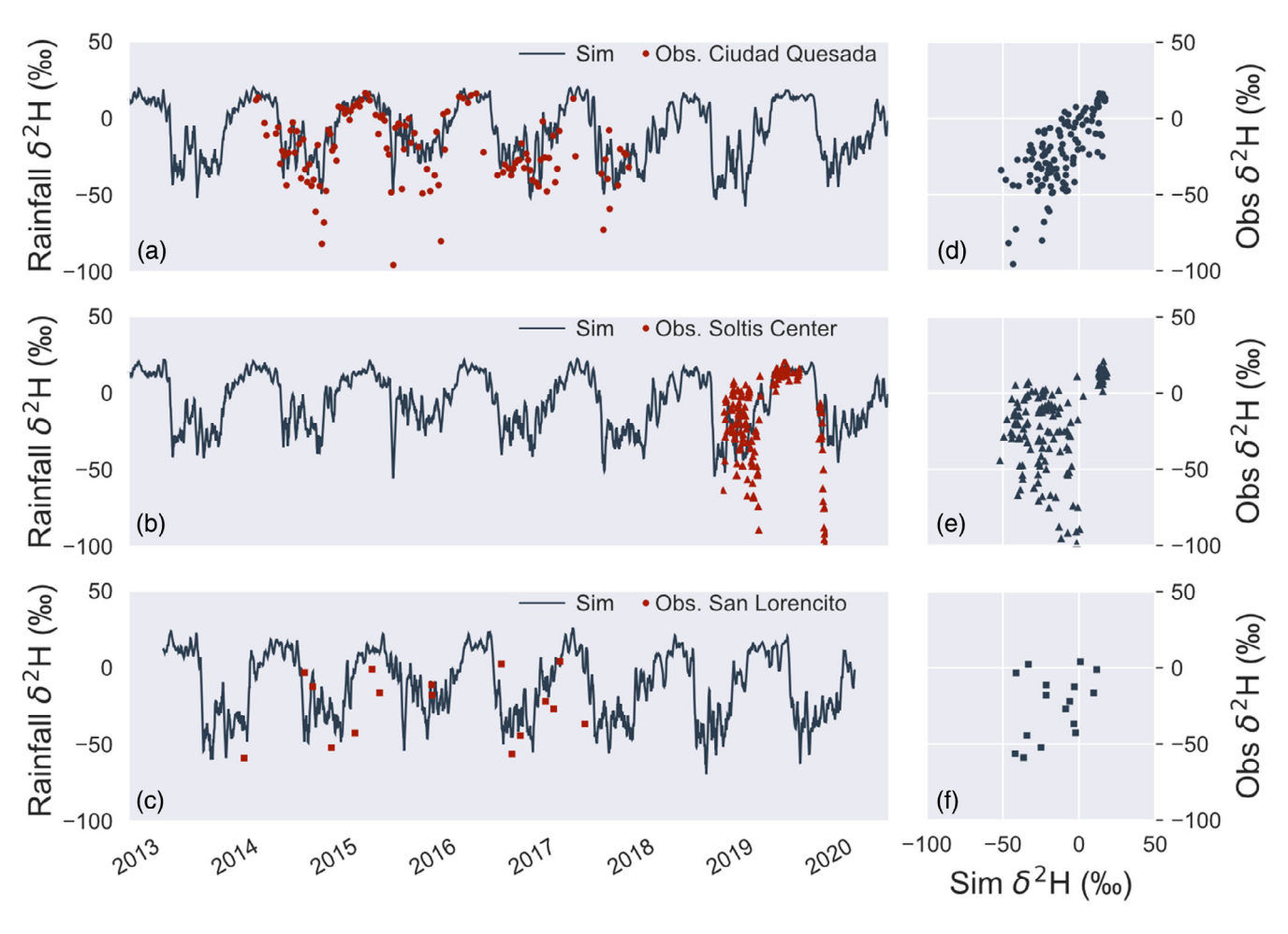


FIGURE 3 Simulated bias-corrected IsoRSM precipitation isotope (deuterium $-^2$ H) data plotted against available observed isotope data at three measurement stations.

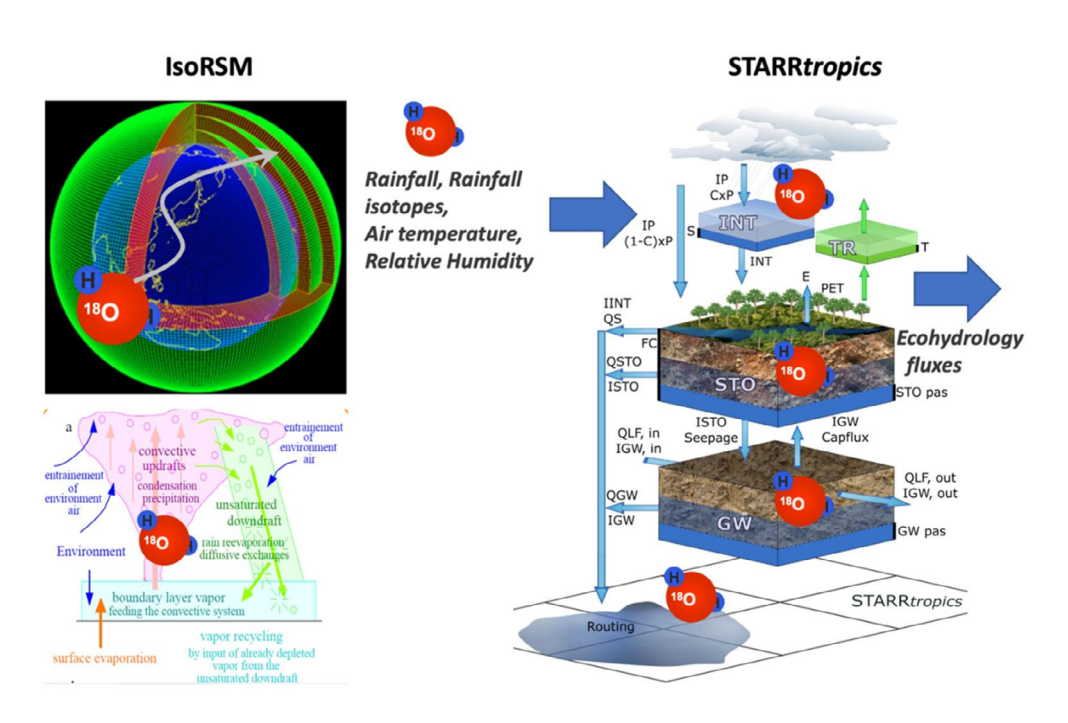


FIGURE 4 Conceptualization of how the isotope-enabled regional climate model (IsoRSM; Yoshimura et al., 2010) output feeds into the ecohydrology model STARRtropics (Correa et al., 2020). The IsoRSM was previously tested for the Central America and Caribbean domain on a 25×25 km grid and resolves major atmospheric processes with isotope transport and fractionation due to water phase changes.

10991085, 2023, 5, Downloaded from https://onlinelbrary.wiley.com/doi/10.1002/hpp.14884, Wiley Online Library on [0.1052022]. See the Terms and Conditions (https://onlinelbrary.wiley.com/terms-and-conditions) on Wiley Online Library for rules of use; OA articles are governed by the applicable Creative Commons License

of the San Lorencito. The development involved implementing a modified LAI-based Rutter interception and a runoff generation routine (Dehaspe et al., 2018) and isotope-based ecohydrological water partitioning into STARRtropics (Correa et al., 2020). We then tested different spatial and temporal resolutions for the STARRtropics application to the 2565 km² San Carlos catchment with four land use classes (forest, pasture, crop, and urban). Here, we settled on a 1-km grid scale and daily model time step as this was able to differentiate catchment physical characteristics in terms of topography and land use; but still adequately account for the observed hydrological response time of around 1 day for the entire catchment. The STARRtropics conceptual runoff generation approach used six calibrated parameters (FC1 and FC2, BetaSeepage, kS, kG, and Ksat) and was loosely based on the two-reservoir HBV model conceptualization of Seibert and Vis (2012). The parameters FC1 and FC2 differentiate TWI-based hillslope from valley runoff generation independent of land use. Land use was assumed to mostly influence interception and water partitioning reflected in the spatially distributed LAI input map (Correa et al., 2020). Additionally, to the six runoff generation parameters, the model included two calibrated interception parameters (Ds, b), three calibrated tracer mass balance parameters (GWpas, Smpas1, and fracSM), and three parameters (ttmp, cevp, and cevpam) for potential evapotranspiration using the default temperature-based method implemented in the HYPE model (Lindström et al., 2010). The total number of 14 calibrated model parameters with a short description and initial ranges can be found in Table 2. The tracer module couples isotope transport and mixing to water fluxes using a mass balance approach. Tracer damping is achieved with additional calibrated mixing volume parameters per model reservoir, which do not hydraulically contribute water to the stream. Both, the dynamic and hydraulically active storages (SM, GW) together with the associated passive mixing storages (GWpas, Smpas1) result in the total catchment storage (Table 2). The total catchment storage is used to calculate monthly residence times (RT) and mean residence times (MRT) as the ratio of total catchment storage to total outflow as the sum of discharge (Qt) and actual evapotranspiration (AET). The latter simple indicators of the study catchment time domain were used due to less computational demand instead of a fully distributed flux tracking approach as in Correa et al. (2020). Furthermore, partitioning of evapotranspiration into transpiration, interception evaporation and soil evaporation followed Correa et al. (2020) and an isotope mass balance approach together with the Craig-Gordon model (Gonfiantini et al., 2018) to compute the isotopic composition of the un-observed evaporating flux with respect to the residual interception and soil store isotopic composition. The major assumptions behind this mass balance approach are that transpiration is a non-fractionating process (the transpired isotopic water composition equals the soil water isotopic composition), that the Craig-Gordon derived evaporative fractionation depends on the relative humidity and air temperature, that the ambient water vapour isotope composition is in equilibrium with rainfall and that the transpiration rates cannot exceed total actual evapotranspiration (Correa et al., 2020; Gonfiantini et al., 2018). The latter isotope mass balance approach can theoretically fail, for example, in

case of more enriched evaporating waters with respect to the atmospheric water vapour isotope composition, if the evaporating soil water source is enriched relative to the atmospheric water vapour source (=precipitation), which we did not observe with this data set.

3.2.1 | Temporal model evaluation

We generated 10 000 Monte Carlo, randomly sampled, parameter combinations for the period from 1985 to 2018 (Table 2). The previous first 2 years, from 1983 to 1984, were used as a model warm-up period that proved sufficient to equilibrate storage levels and not included in the calibration process. The longest available streamflow record at the Terron Colorado station (Table 2) was split in a calibration (1984–1997) and validation (1998–2003) period. Then, the simulations were jointly evaluated using the Kling-Gupta Efficiency (KGE) and Nash-Sutcliffe-Efficiency (NSE) criteria for discharge (Qt), correlation coefficient (CC) for streamwater isotopes (QconcT) as calibration targets, and the Mean Absolute Error (MAE) for the independent model evaluation using measured transpiration in a model pixel to point-scale comparison.

The discharge scores KGE and NSE were averaged using 0.7^* Terron Colorado + 0.1^* Boca Tapada + 0.1^* Jabillos + 0.1^* Pocosol with a greater relative weight for the largest downstream station Terron Colorado because it had the longest 30-year gauged daily record (Figure 1 for station locations). The monthly streamwater isotopes used a correlation coefficient as a criterion to evaluate the isotope dynamics due to a relatively lower number of observations (<12) that result in insensitive KGE or NSE performance. The calibration targets were KGE_Qt > 0.4, NSE_Qt > 0.2, and CCQconcT > 0.3, and only simulations that exceeded these thresholds were deemed acceptable and retained for further analysis and a qualitative uncertainty assessment. The accepted parameter sets were analysed for spatio-temporal ecohydrological water partitioning, storage, discharge, and isotope simulations.

3.2.2 | Spatial model evaluation

The accepted parameter sets were used to simulate spatial maps of isotope compositions of components of ecohydrological water partitioning, associated fluxes and storage dynamics. Spatial model output was generated for an average ensemble of the retained 52 best simulations and then aggregated to mean annual values of total catchment storage (active plus passive storage), soil storage isotope composition, groundwater storage isotope composition, mean residence time, ratio of transpiration to precipitation (Transp/P) and ratio of transpiration to actual evapotranspiration (Transp/AET). Available point-scale measurements (soil and groundwater isotope composition) and modelled estimates (MRT, Transp/AET) were used for an independent model evaluation. The latter estimates were independently compared against measured groundwater isotopes from Sánchez-Murillo and Birkel (2016), flux tracking transit time estimates by Correa et al. (2020) and



TABLE 2 Prior parameter ranges used for a total of 10 000 Monte Carlo parameter sampling iterations.

	•	_	· · · · · · · · · · · · · · · · · · ·		
Parameter	Units	Process	Description	Min	Max
Ds	mm/d	Routing	Drainage from canopy when the storage is completely filled	0.1	2.8
b	-	Routing	Exponent in Rutter interception module	3.8	4.8
FC1	mm	Storage	Water holding capacity of the soil in hillslopes	200.0	500.0
FC2	mm	Storage	Water holding capacity of the soil in valleys	500.0	700.0
BetaSeepage	-	Runoff	Non-linear exponent for soil store runoff generation	0.4	3.5
ks	1/d	Baseflow	Recession coefficient of discharge from soil store	0.002	0.3
kG	1/d	Baseflow	Recession coefficient baseflow	0.001	0.1
Ksat	mm/d	Groundwater	Horizontal saturated hydraulic conductivity	1.0	200.0
GWpas	mm	Groundwater	Additional (passive) groundwater mixing volume	140.0	1000.0
SMpas1	mm	Isotopes	Additional (passive) soil mixing (SM) volume	40.0	270.0
fracSM	-	Isotopes	Scaling factor for SM volume	0.4	0.9
ttmp	°C	Evapotranspiration	Threshold temperature for evapotranspiration	8.0	9.7
cevp	mm/°C.d	Evapotranspiration	Evapotranspiration parameter	0.25	0.35
cevpam	-	Evapotranspiration	Amplitude of sinus function that corrects potential evapotranspiration	0.25	0.35
•	mm/°C.d -		Amplitude of sinus function that corrects potential		

Note: Wide initial parameter ranges were informed by previous work (Correa et al., 2020; Dehaspe et al., 2018), and we kept parameter names identical to previous publications and, therefore only a short description is included.

Birkel et al. (2021), measured transpiration by Aparecido et al. (2016), and independently modelled transpiration estimates by Iraheta et al. (2021).

4 | RESULTS

4.1 | Temporal simulation of isotope and ecohydrological processes and model performance

Assessing the model parameter identifiability after 10 000 MC sampling iterations showed the most identifiable parameters in terms of influencing the performance criteria were kS, kG, Betaseepage, SMpas1, cvep, and ttmp. The first three parameters control the hydrologic response of the upper (kS) and lower (kG) model reservoir with the Betaseepage parameter-controlled water distribution from the soil storage into runoff generating storage and evapotranspiration of available water. The mixing volume SMpas1 damps the incoming isotopic variability. The parameters cvep and ttmp were sensitive to simulated water partitioning and evapotranspiration (Figure 5). However, we also found runoff generation parameters (e.g., kS) that influence tracer transport and mixing (e.g., SMpas1 parameter in Figure 5—Isotopic sensitivity panel).

The overall maximum scores for streamflow from the 10 000 MC simulations were $\sim\!\!0.6$ for KGE and $\sim\!\!0.28$ for NSE, streamflow isotopes showed a maximum CC of $\sim\!\!0.48$, and transpiration a minimum MAE of 1.34 mm (range from 1.34 to 1.64 mm); however, only 52 simulations preserved a balanced performance (Figure 6) satisfying all calibration targets and were further used to analyse large-scale ecohydrological water partitioning.

Overall, daily discharge dynamics were reasonably simulated, with KGE values ranging from 0.31 to 0.73 for individual timeseries for all accepted parameter sets and at all gauging stations (Figure 7). Model performance increased with catchment scale and was best at the most downstream station Boca Tapada (max KGE = 0.73) and lowest at the upstream Pocosol gauging station (142 km²) with maximum KGE values of 0.48. The simulations captured the discharge seasonality with less flow from January to March (dry season) and the high flow period with peaks in September and October (second leg of the rainy season forced by the ITCZ and synoptic systems). The water balance was correctly simulated, but the model was less successful in capturing peak flow events likely due to model input, spatial data, model structure and parameter uncertainty. The latter was reflected in lower NSE values of around 0.3 (Table 3). The timings of low flow and drought periods were correctly simulated, albeit with a trend towards underestimation (see log-scale discharge in Figure 7). The calibration period covered was long enough to capture interannual variability with several records for extreme events such as among others Hurricane Joan in 1988, the above-average hurricane season in 1995, the record discharge drought in 1997-1998 due to El Niño, Hurricane Otto in 2016, tropical storm Nate in 2017, and another record low flow period in 2018-2019 reported by Birkel et al. (2020) and linked to the 2015-2019 extended drought visible in the annual mean water balance of Figure S2 (Pascale et al., 2021).

Similarly, the streamwater isotope range was reasonably simulated at most observed streams (mean CC \sim 0.35). Figure 8 depicts a slightly better performance at the stream sites ID 31 (e.g., catchment area of 96 km²) and ID 7. The isotope simulations at larger stream sites such as site ID 41 that corresponds to the Boca Tapada downstream gauging station with an area of 2413 km² resulted less

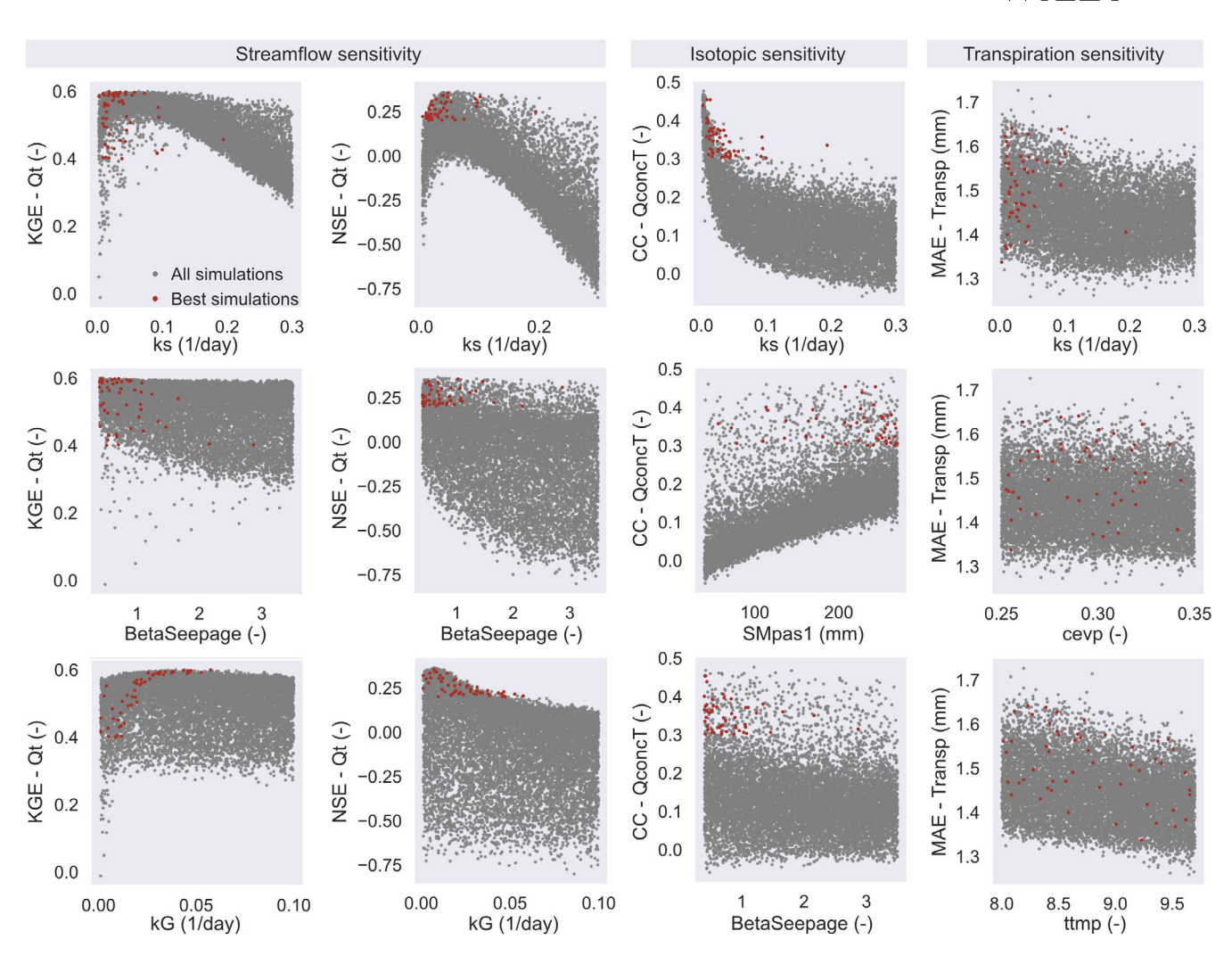


FIGURE 5 Identifiable parameters compared against different objective functions. The most identifiable runoff generation parameters BetaSeepage, kS, and kG plotted against KGE and NSE. Isotope parameter SMpas1 is plotted against the CC (correlation coefficient), and the evapotranspiration routine parameters cevp and ttmp are visualized against the MAE of transpiration. Red dots correspond to the 52 best simulations that satisfied the imposed calibration target.

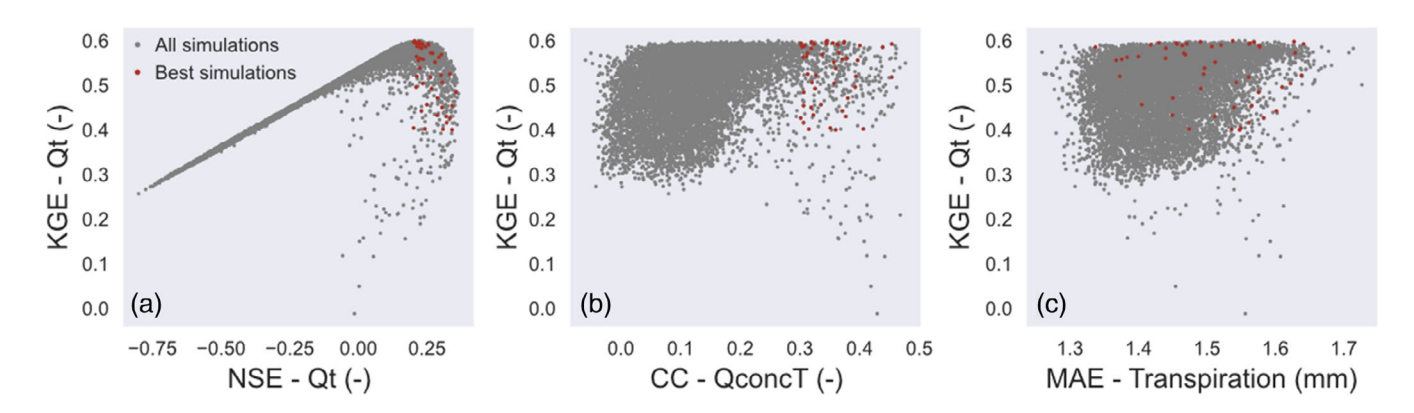


FIGURE 6 Summary of all scores (KGE, NSE, CC, and MAE) with respect to the 52 best simulations that satisfied the imposed calibration target (red dots).

dynamic and more seasonal compared to more variable headwater streams such as site ID 31 with more simulated isotope peak events (Figure 8). However, the short and monthly stream isotope sampling precluded from a more systematic temporal model evaluation. The model was not able to simulate the observed isotope lapse rate visible from the stream deuterium samples (Figure S1a), with only more

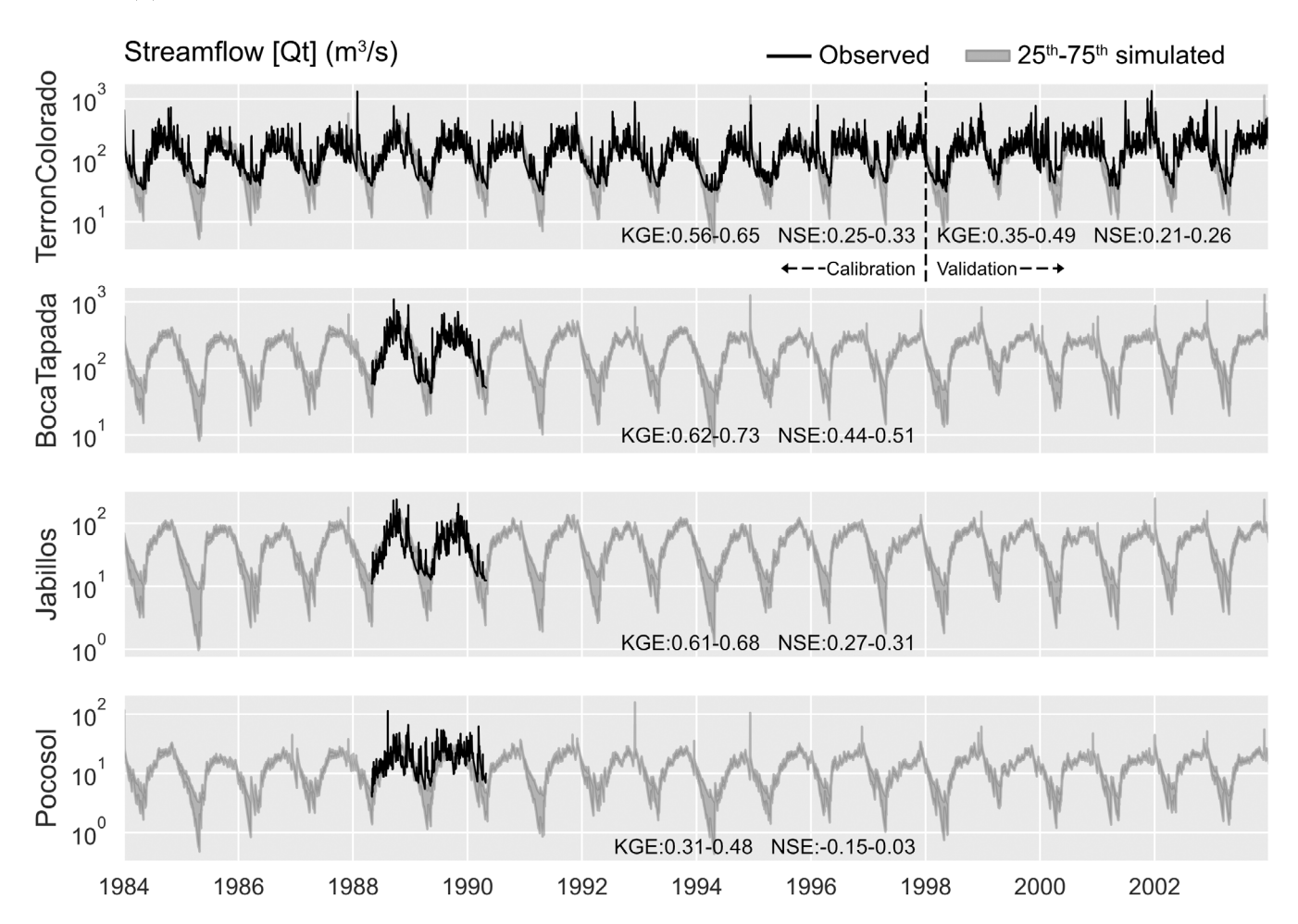


FIGURE 7 Observed discharge (black line) plotted against the log-scale interquartile range (25th-75th) of the 52 accepted simulations from 1984 to 2003 with an indication of the full range of KGE and NSE performance criteria.

depleted simulated isotope compositions at the highest mean catchment elevations. Such a mismatch in gradient was driven by the rainfall isotope input data, where the more depleted rainfall events were additionally underestimated by IsoRSM (Figure 3).

The retained model simulations were then used to quantify catchment-scale ecohydrological water partitioning and storage dynamics. The aggregated monthly simulations indicated seasonal AET and storage dynamics driven by rainfall patterns (Figure 9a). The annual aggregated annual simulations are shown in Figure S2 and Table S1 in the Supplementary Material. Average modelled total catchment storage (dynamic plus passive subsurface and groundwater storage estimated by STARRtropics) oscillated around 1200 mm, with normalized storage of 0.4 with respect to minimum and maximum storages (Figure 9c, Figure S2c). The storage percentiles 25th and 75th were computed as 1100 and 1370 mm, which correspond to 0.2 and 0.6 of the normalized storage, respectively. The model reproduced monthly storage of about \sim 1200 mm and remarkable low monthly discharge (~200 mm) events during the wet season in the years 2009-2010 and 2018 (Pascale et al., 2021). Similarly, the evapotranspiration signal showed a pronounced seasonality over the complete period, with the simulated AET being close to 70% compared to PET (Figure S2e), and 66% at the annual scale (Table S1). Furthermore, the temporal pattern was shifted with a maximum AET close to 100 mm at the beginning of the rainy season, in contrast to PET with maximum values during the driest months. The latter peak AET was explained by peak transpiration (transp) due to higher radiation inputs and sufficient soil water availability. For the whole simulation period, the maximum transpiration also resulted in maximum transp/AET ratios close to 1 during the peak rainfall months in June and October and with minimum values as low as 0.01 during dry months in April and May (Figure 9k). The monthly residence time indicator (i.e., the total storage to sum of discharge ratio and actual evapotranspiration) closely followed the hydroclimatic seasonality with shorter RTs over the rainy season in the order of around 6 months which increased up to 5 years over the driest months for some drought periods on record (Figure 9l). Increasing RTs were qualitatively detected since 2010 due to a decrease in rainfall inputs (Figure 9a,f, Figure S2a).

4.2 | Spatial simulation of isotope and ecohydrological processes and independent model evaluation

Modelled total (active plus passive) storage estimates ranged from 1000 to 2000 mm for over 90% of the grid cells in the catchment

TABLE 3 Posterior parameter statistics (mean, standard deviation, minimum, and maximum) of the retained 52 simulations.

Parameter	Units	Process	Mean	Std	Min	Max
Ds	mm/d	Routing	1.22	0.79	0.14	2.70
В	-	Routing	4.34	0.29	3.83	4.79
FC1	mm	Storage	356.45	92.08	200.45	499.65
FC2	mm	Storage	603.54	59.53	503.04	699.54
BetaSeepage	-	Runoff	0.79	0.46	0.40	2.87
Ks	1/d	Baseflow	0.04	0.033	0.00	0.19
kG	1/d	Baseflow	0.02	0.01	0.00	0.06
Ksat	mm/d	Groundwater	73.08	52.56	2.59	191.49
GWpas	mm	Groundwater	578.22	245.99	152.27	962.37
SMpas1	mm	Isotopes	213.35	57.25	56.61	269.45
fracSM	-	Isotopes	0.71	0.13	0.43	0.89
Ttmp	°C	Evapotranspiration	8.77	0.52	8.01	9.65
Cevp	mm/°C	Evapotranspiration	0.31	0.03	0.25	0.35
cevpam	-	Evapotranspiration	0.29	0.03	0.25	0.34
KGE Qt	-	Kling-Gupta for discharge	0.59	0.06	0.55	0.63
NSE Qt	-	Nash-Sutcliffe for discharge	0.28	0.06	0.24	0.32
LogKGE Qt	-	KGE for logarithm of discharge	0.56	0.18	0.12	0.77
LogNSE Qt	-	NSE for logarithm of discharge	0.31	0.33	-0.6	0.65
CC QconcT	-	Correlation coefficient of streamwater isotopes	0.35	0.04	0.30	0.45
MAE Transp	mm	Mean absolute error for transpiration	1.51	0.08	1.34	1.64

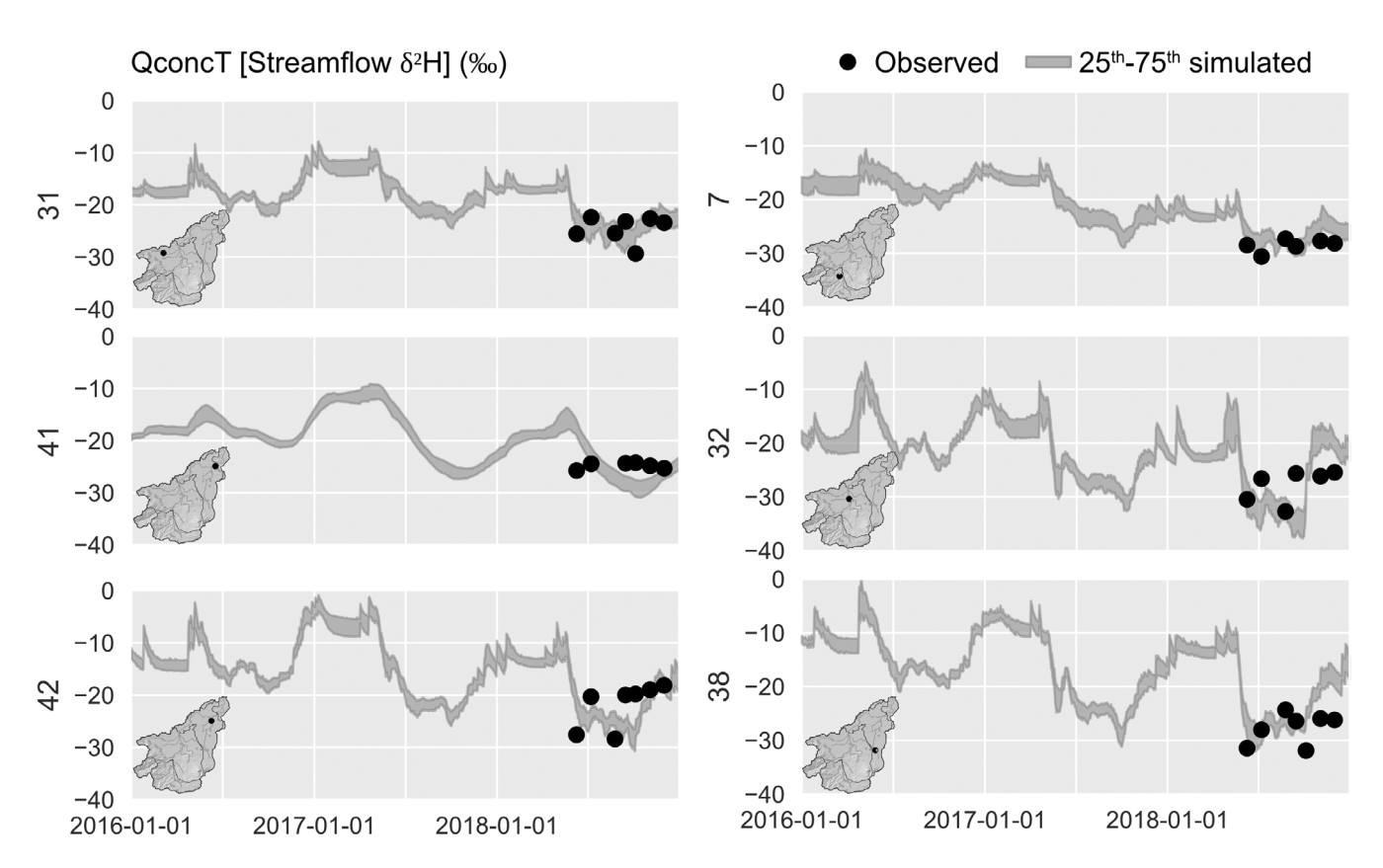


FIGURE 8 Observed monthly average streamwater δ^2H plotted against the interquartile range (25th–75th) of the 52 retained simulations at selected monitoring points throughout the catchment representing upland (7, 31 38) and lowland (32, 41, 42) sites from 2016 to 2018.

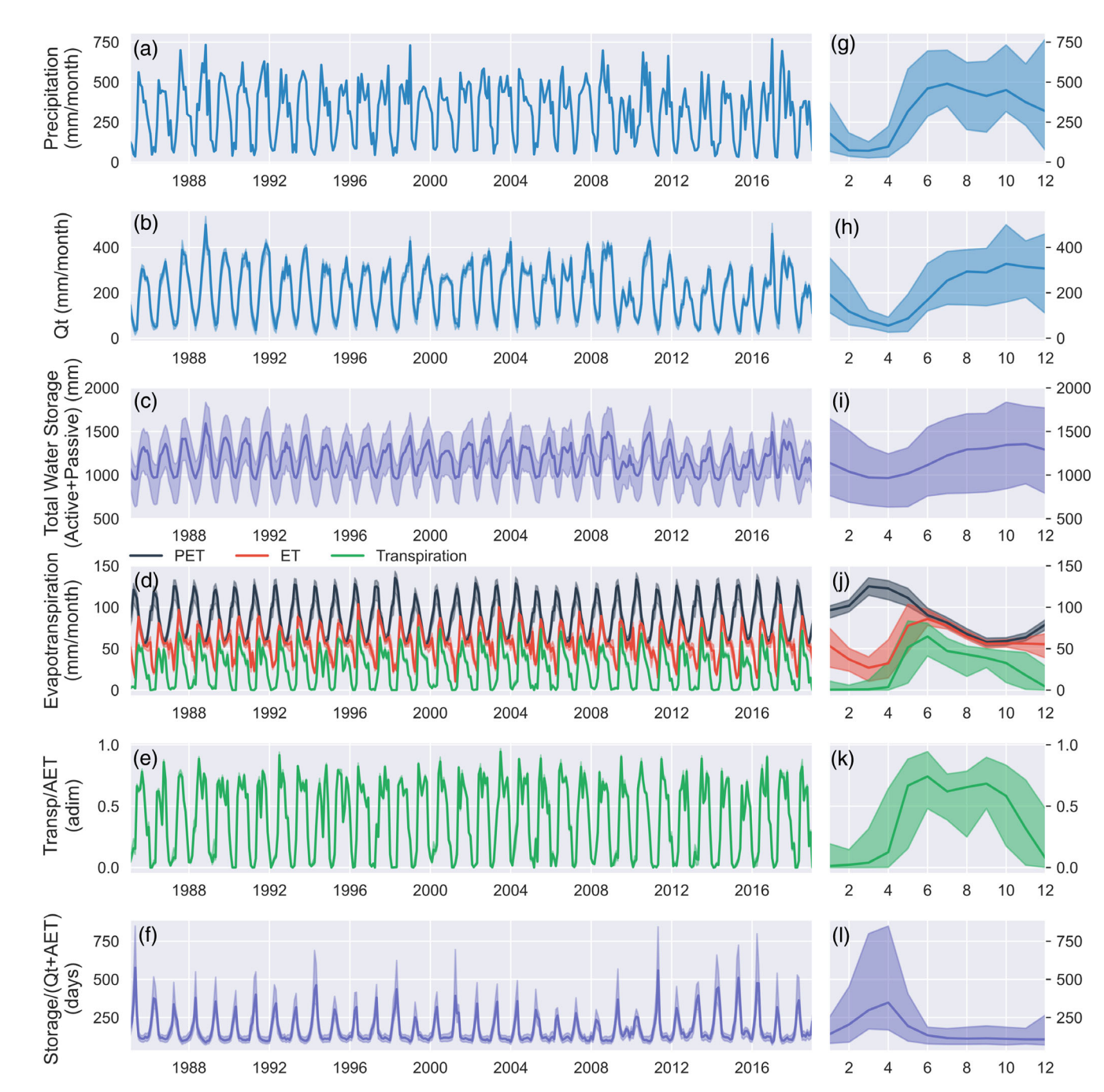


FIGURE 9 Modelled catchment scale average and monthly resampled and mean monthly water fluxes (a, g) precipitation, (b, h) discharge at the San Carlos catchment outlet, (c, i) total storage, (d, j) AET partitioning, (e, k) Transp/AET series, and (f, l) residence times as storage/(Qt + AET) are visualized as the interquartile 25th-75th bands of the retained 52 best simulations.

(Figure 10a, Table S1). However, somehow counterintuitive, higher modelled storage accumulated in the headwaters down to around 1000 m.a.s.l., with the lowlands showing less and uniform modelled storage capacity, which is related to the simplification used in STARR to simulate lateral flow as a function of the slope of the terrain (Dehaspe et al., 2018). Average soil and groundwater isotope composition exhibited a spatial gradient related to the precipitation and streamflow isotopic lapse rate (Figure S1b). The further away from the Atlantic coast and the higher the elevation resulted in a more depleted

isotope composition, with simulations generally reflecting the 30 (<30 m depth) monitored shallow groundwater wells (-18% to -54%, deuterium with a CC = 0.72) and the measured average point soil isotope (-23% deuterium, Figure 10b) composition at San Lorencito. The observed and simulated groundwater isotope composition showed a CC of 0.7 and generally follow a 1:1 trend (Figure 10c); however, enriched isotope signatures were under-estimated by 5‰-10‰ and the more depleted headwater groundwater isotope composition was over-estimated by 10‰, presumably due to under

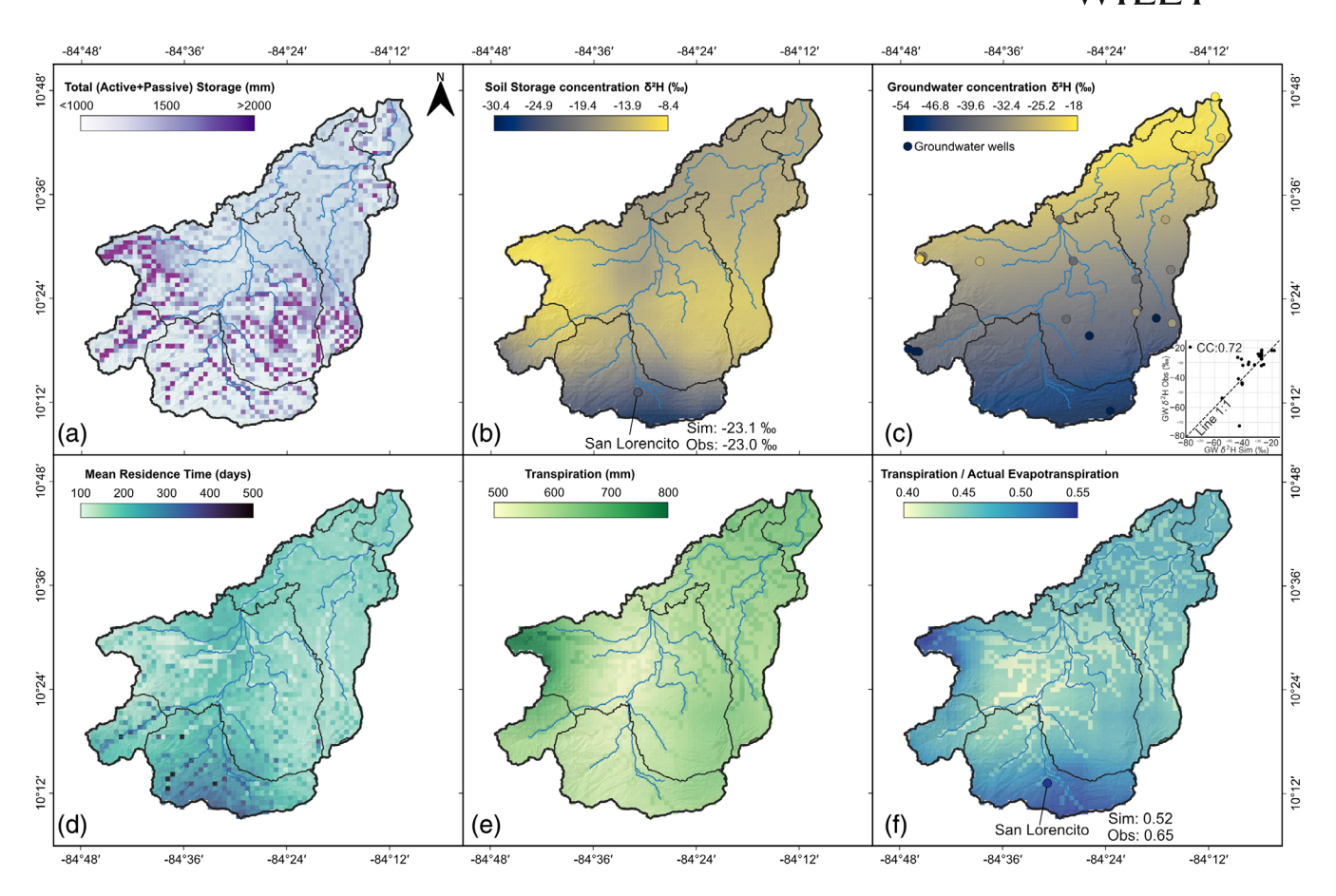


FIGURE 10 Mean annual maps (1985–2018) of simulated average (a) total catchment storage, (b) soil storage isotope composition, (c) groundwater storage isotope composition and correlation between observed and modelled isotope composition, (d) mean residence time (MRT), (e) transpiration (Transp) and (f) transpiration/actual evapotranspiration (Transp/AET). Measured groundwater isotope composition was superimposed on (c) and point-scale soil isotope measurements (b), MRT (d), and Transp/AET estimates (f) at San Lorencito for independent model evaluation.

estimation of depleted heavy rain events recharging aquifers. The soil isotope pattern additionally featured more enriched compositions in the higher rainfall areas. Further, the observed streamflow isotope lapse rate was not reproduced by the model compared to an improved groundwater isotope lapse rate (Figure S1a). The estimated MRTs reflected the average spatial rainfall pattern with the shortest residence times in areas with higher accumulated rainfall and steeper terrain (the northwestern and southeastern parts of the San Carlos, Figure 1a,e). The San Lorencito experimental catchment area yielded mean transit times estimates of around 2–4 years. The simulated average ecohydrological water partitioning showed higher average Transp/AET and lower Transp/P ratios in the aforementioned areas of higher rainfall and lower AET.

STARRtropics simulated mean annual ecohydrological water partitioning from around 0.43 to 0.5 for the Transp/AET ratio, from 0.31 to 0.43 for the AET/P ratio and from 0.14 to 0.19 for the Transp/P ratio (Table 4). The Transp/AET ratio showed relative similarity among the modelled land use classes with crops such as sugar cane or pine-apple resulting in lower Transp/AET compared to the higher Transp/AET of forest and grass. The Transp/AET ratios for forests across the catchment resulted relatively similar. Further, the Transp/AET ratios

increased from 0.45 in the lowlands to 0.5 in the headwaters. However, Transp/P decreased with large precipitation rates (around 4150 mm in the high elevations to the west and east of the catchment) and decreasing AET (1421 to 1225 mm) with elevation (Table 4). The LAI affects the Transp and AET estimates due to the LAI-driven net precipitation (Dehaspe et al., 2018), where the Transp/AET ratio decreased from 0.48 to 0.43 with increasing TWI in the central catchment area characterized by lower LAI values associated to agricultural land use (Figure 1b,e).

5 | DISCUSSION

5.1 | Value of isotope integration and multi-criteria calibration for upscaling a conceptual ecohydrological model

Process-based hydrological modelling at larger scales is a major challenge as small-scale hydrological process descriptions often represented by model parameters are often scale-dependent (Bashford et al., 2002). This scale dependency is true for most models from

TABLE 4 Zonal statistics of ecohydrological fluxes and signatures (P, AET, Transp, AET/P, Transp/P, Transp/AET) by land use class, elevation zones, and TWI classes (as in Figure 1).

Land use	Area (%)	Prec (mm/year)	AET (mm/year)	Transp (mm/year)	AET/Prec (-)	Transp/AET (-)	Transp/Prec (-)
Grass	21.68	3857 ± 718	1295 ± 102	609 ± 45	0.34 ± 0.05	0.47 ± 0.03	0.16 ± 0.02
Forest	44.6	3866 ± 768	1296 ± 102	613 ± 45	0.34 ± 0.05	0.47 ± 0.02	0.16 ± 0.02
Crops	23.94	3619 ± 525	1307 ± 77	589 ± 41	0.37 ± 0.04	0.45 ± 0.02	0.16 ± 0.02
Urban	1.67	4007 ± 631	1311 ± 78	599 ± 40	0.33 ± 0.05	0.46 ± 0.03	0.15 ± 0.02
Bare ground	1.43	3786 ± 851	1309 ± 100	603 ± 62	0.36 ± 0.05	0.46 ± 0.03	0.16 ± 0.02
Water	0.39	3388 ± 318	-	-	-	-	-
Pineapple	4.49	3519 ± 263	1341 ± 58	602 ± 21	0.38 ± 0.02	0.45 ± 0.01	0.17 ± 0.01
Cane	1.8	3389 ± 462	1281 ± 63	559 ± 33	0.39 ± 0.04	0.44 ± 0.01	0.17 ± 0.01
Elevation (m.a.s	s.l) Area (%	6) Prec (mm/year)	AET (mm/year)	Transp (mm/year)	AET/Prec (-)	Transp/AET (-)	Transp/Prec (-)
0 to 400	59.5	3579 ± 442	1329 ± 99	601 ± 43	0.38 ± 0.04	0.45 ± 0.02	0.17 ± 0.02
400 to 800	14.3	4342 ± 836	1304 ± 113	616 ± 69	0.31 ± 0.04	0.47 ± 0.03	0.14 ± 0.02
800 to 1200	13.2	3885 ± 964	1225 ± 120	600 ± 43	0.33 ± 0.05	0.49 ± 0.03	0.16 ± 0.03
1200 to 1600	8.0	3888 ± 841	1227 ± 98	608 ± 29	0.33 ± 0.04	0.50 ± 0.02	0.16 ± 0.03
1600 to 2200	5.0	4148 ± 631	1255 ± 56	625 ± 11	0.31 ± 0.03	0.50 ± 0.02	0.15 ± 0.02
TWI ranges	Area (%)	Prec (mm/year)	AET (mm/year)	Transp (mm/year)	AET/Prec (-)	Transp/AET (-)	Transp/Prec (-)
9 to 11.5	10.14	4343 ± 834	1283 ± 94	617 ± 50	0.30 ± 0.04	0.48 ± 0.02	0.15 ± 0.02
11.5 to 14	47.14	3846 ± 732	1259 ± 92	602 ± 46	0.33 ± 0.04	0.48 ± 0.03	0.16 ± 0.02
14 to 16.5	30.15	3618 ± 569	1322 ± 111	603 ± 46	0.37 ± 0.04	0.46 ± 0.03	0.17 ± 0.02
16.5 to 19	7.36	3581 ± 415	1421 ± 84	611 ± 43	0.40 ± 0.03	0.43 ± 0.02	0.17 ± 0.01
19 to 25	5.21	3312 ± 258	1416 ± 86	613 ± 52	0.43 ± 0.02	0.43 ± 0.01	0.19 ± 0.01

Note: The area is the percentage of land use class, elevation zone, or TWI class to total catchment area. Statistics correspond to the mean \pm SD.

simple to complex (Beven, 1995), which can cause problems simulating runoff generation and ecohydrological processes at larger catchment scales. Smith et al. (2021) recently applied the physically-based, tracer-aided EcH2O-iso ecohydrology model, which was mostly developed for small experimental catchments of a few km² by Kuppel et al. (2018), in a drought-sensitive, lowland mesoscale catchment $(\sim 70 \text{ km}^2)$ in Germany, testing different spatial grid scales. They found that a spatial aggregation of >1 km² grid size was no longer suitable to reliably represent runoff generation and flow routing with associated tracer mixing, resulting in over-averaged discharge and tracer responses. In our wetter, tropical and higher relief catchment setting, we settled on a 1-km pixel size resolution and a daily model time step. This configuration was still able to reproduce the topographydominated (STARRtropics uses the TWI to generate and route flow similar to the original TOPMODEL approach of Beven & Kirkby, 1979) discharge response to rainfall events (Figures 7 and 8) and also the associated tracer mixing and transport at a greater computational efficiency, but at the expense of lower performance at more dynamic headwater sites such as, for example, the San Lorencito experimental catchment simulated by Dehaspe et al. (2018) and Correa et al. (2020). Discharge simulations at the outlet of the San Carlos catchment were similar to other conceptual modellings, such as the regionally calibrated HYPE model for Costa Rica (Arciniega-Esparza et al., 2022), with a KGE and CC of 0.61 and 0.91.

Temporal model parameter dependencies (Reusser et al., 2011) could not be considered due to the computational demand of the fully distributed STARRtropics and large-scale model domain. However, the multi-criteria temporal model evaluation used time series from a unique data set of discharge and monthly streamwater isotopes evaluated at 46 sampled rivers with a combined NSE, KGE and CC calibration target. We did not perform an exhaustive test comparing many different statistical calibration criteria such as in Stadnyk and Holmes (2020), but the most sensitive criterion evaluating a balanced model able to represent the complete range of discharge was the KGE. We used correlation coefficients as a calibration target for streamwater isotopes as we had few available observations, which was also found to be a reasonable approach by Stadnyk and Holmes (2020), but should be changed to using KGE for calibration with more observations in the future. Further, evaluating simulated transpiration and observed groundwater isotope composition as an independent model test, helped gain insights into model limitations (Figure S1b), which mostly point towards the need to improve spatially and temporally distributed model inputs and data for evaluation.

For example, the ecohydrological water partitioning in STARRtropics depends on the LAI as indicator of vegetation density and a simplified Rutter interception routine with only two parameters. The latter worked well at the small 3.2 km² experimental headwater catchment scale with a relatively homogeneous pre-montane rainforest

(Dehaspe et al., 2018), but required other un-tested land cover types (urban, crops, etc.) additionally to forest for the Rutter model parameters at the larger scale. Furthermore, the spatially variable but temporally constant LAI used here is subject to greater variability over such a mixed land use catchment and over 30 years of simulated fluxes; however, the lack of LAI datasets from 1980 to 2000 complicates the evaluation of the long-term vegetation dynamics and changes related to land use. Additionally, the internal isotope mass balance used to calculate transpiration from net precipitation after interception (after Correa et al., 2020) depends on the spatial rainfall isotope variability IsoRSM output, which resulted rather homogeneous over parts of the model domain with different land use classes. Consequently, we derived relatively similar transpiration fluxes for grass and forest and different crops such as pineapple and sugarcane located in close proximity (Table 4). Additionally, the IsoRSM simulated precipitation isotopes underestimated the actual day-to-day isotopic variability in the region resulting in underestimated peak event streamwater isotopes.

Therefore, the largest source of uncertainty and challenge in modelling was the distributed input data to drive the model (e.g., underestimation of peak rainfall events by global products as demonstrated by Arciniega-Esparza et al., 2022). Nonetheless, few such attempts to use climate model output as drivers for tracer-aided hydrological modelling have been made in the past (e.g., Delavau et al., 2017 for a large catchment in Canada), but in the future, this might be the only feasible approach to generate large-scale ecohydrological simulations of water partitioning, particularly in scarce data regions. Much needed reduced climate model uncertainty might depend on finer-scale water isotope simulations of the soil-atmosphere moisture recycling feedback as well as in-cloud processes (Yoshimura, 2015).

5.2 | Spatio-temporal model realism across a tropical catchment gradient

Independent model evaluation with spatially distributed data, pointscale measurements and model estimates attempted to evaluate model realism of STARRtropics in terms of reasonable water partitioning, discharge, storage, and isotope simulations. We compared the groundwater isotope simulations with 30 measured shallow groundwater wells (max 30 m depth) from Sánchez-Murillo and Birkel (2016) with an average CC of 0.72 (Figure 10c). The model picked up on the isotope lapse rate in groundwater of more depleted isotope compositions at higher elevations but failed to simulate the streamflow isotope lapse rate (Figure S1a). The groundwater simulations reflected potential preferential groundwater recharge that results in more depleted groundwaters compared to average rainfall and streamwater isotope compositions pointing at active recharge during the highest, most intense and isotopically most depleted rainstorms in September/ October (Jasechko & Taylor, 2015; Sánchez-Murillo et al., 2020; Sánchez-Murillo & Birkel, 2016). Soil water isotope simulations matched point-scale averaged soil water isotope measurements from the San Lorencito experimental catchment, albeit we recognize such a single

point measurement does not reflect the naturally occurring soil water isotope variability (Figure 10b). More complex simulated transpiration for the matching grid cell of the Soltis research site showed comparable average measured transpiration within a range of MAE from 1.34 to 1.64 mm with underestimated modelled peak transpiration and only subtle differences in AET partitioning across modelled land uses and topography (Table 4). Further, the model overemphasized the transpiration seasonality (Figure 9) compared to relatively homogeneous all-year measured transpiration of the pre-montane rainforest at Soltis (Moore et al., 2018). The latter likely resulted from the relatively simple temperature-driven PET model that was used as a basis to partition AET into evaporation and transpiration and finally overestimating simulated AET (Mueller & Seneviratne, 2014). As a result, our simulated overall Transp/AET ratios of 0.44 to 0.5 (Table S1) were on the lower side compared to global estimates for the tropics (e.g., Wei et al., 2016). Interestingly, the STARRtropics-simulated transpiration of the San Lorencito experimental catchment (Figure 10d) by Correa et al. (2020) with Penman-Monteith PET resulted in slightly higher Transp/ET ratios (avg 0.65 compared to 0.5 from the largescale model) with overall less than half (~350 mm/year) of the simulated annual transpiration flux from the large-scale model (~600 mm/ year. Table 4). The large-scale transpiration flux estimates for the San Carlos of Iraheta et al. (2021), based on a simple mean annual and monthly isotope mass balance model, were in the same range of around 600 mm/year compared to the STARRtropics simulations. However, their Transp/ET ratios up to 0.8 were also higher than the model results here. Despite differences and method-dependent uncertainties surrounding the absolute values of ET partitioning, all estimates by Correa et al. (2020) and Iraheta et al. (2021) and measurements by Aparecido et al. (2016) generally were consistent with

Previously modelled catchment storage (Correa et al., 2020; Dehaspe et al., 2018) for a few grid cells of the San Lorencito site (variable groundwater storage from a few mm to 600 mm) also agreed with the large-scale STARRtropics model results (Figure 10a). The relatively large storage of around 1000 mm resulted in longer residence time estimates for the headwaters compared to shorter residence times downstream characterized by less lowland storage capacity. Modelled discharge TTs by Correa et al. (2020) ranged from a few hours up to 2 years depending on the hydroclimatic variability, similar to other research from the humid tropics and Costa Rican catchments (Birkel et al., 2016; Mayer-Anhalt et al., 2022). Independent Tritiumderived baseflow MTT resulted in 2.7 years age estimates with an uncertainty range of around 1.5 years (Birkel et al., 2021). Higher storage capacity of headwater catchments at higher elevations compared to lowland catchments was recently shown to be a global feature (Jasechko et al., 2016). However, it is also likely that lowland areas have much higher groundwater storage in fluvial floodplain deposits, which is not connected to surface water drainage and is therefore a volumetric blind spot for the model. Further, differences arise from the calculated total storage consisting of hydraulically active and

our large-scale STARRtropics results within the uncertainty ranges of

measurements

(Coenders-Gerrits

and

models

the

et al., 2014).

different

"tracer-invoked" passive mixing storage (Dehaspe et al., 2018). Higher storage is also related to longer TTs compared to catchments with a faster turnover resulting in a strong global influence of young waters in most catchments (Jasechko et al., 2016). The San Carlos catchment and sub-catchments certainly fall into the young water-dominated catchments category due to high rainfall inputs even if the calculated residence times were around 1 year. The above discussion clearly showed that STARRtropics reasonably simulated hydrological processes at the aggregated catchment scale with some first-order water partitioning and storage estimates that need improvements to be able to simulate more detailed spatial patterns.

MODEL LIMITATIONS AND POTENTIAL **FUTURE RESEARCH NEEDS**

We combined a unique isotope data set (from 46 rivers) and multicriteria calibration to upscale the fully distributed, conceptual traceraided hydrological model STARRtropics to spatial scales beyond 1000 km² (San Carlos catchment) in the Tropics of Central America. Our ecohydrological model provided important and novel insights into water and tracer transport, residence time indicators, as well as the ecohydrological water partitioning across major climate, land use, and topographical gradients. The catchment's response was predominantly driven by high rainfall inputs that override smaller land cover-dependent transpiration fluxes contrary to our initial expectation. The marked topographical gradient (2326 m) resulted in more dynamic but still underestimated water and tracer responses in the headwaters that averaged further downstream also due to underestimated peak rainfall volumes and isotope compositions. Nonetheless, the coarser daily and 1-km pixel headwater simulations suffered compared to more detailed (hourly and 10 m pixel scales) previous model performances; a clear set-back resulting from upscaling to a few 1000 km² catchment scale with necessary aggregation of hydrological processes beyond dynamic small-scale runoff responses of less than 1 h.

The model simulated relatively similar Transp/AET ratios up to 0.5 across different landcover classes with subtle but higher Transp/ AET ratios for forests and grass and lower Trans/AET for crops. The Transp/AET ratios also increased from the lowlands to maximum values in the headwaters, which is likely directly related again to the bias in the model driving variables:

- Rainfall isotope composition was too homogeneous and did not match the observed lapse rate (also emphasized in the simulated streamflow lapse rate), which drives the soil isotope composition used in the mass balance calculating transpiration with relatively small differences among different land covers.
- The time-constant LAI used to partition water into interception, interception evaporation and net precipitation likely underestimates land cover differences.
- The simplistic PET used overestimated evaporation demand contributing to underestimated Tr/AET ratios.

Therefore, albeit a step in the right direction, many challenges remain that need improvements mostly related to input data uncertainty. Despite the prospects of using the output of climate models to drive distributed larger-scale, tracer-aided hydrological models in situations of data scarcity, any such output needs to be downscaled and bias-corrected, which can be a time-consuming task. Furthermore, in future, the ecohydrological water partitioning based on a temporally constant LAI and overly simplistic PET needs to be refined with a time-variable LAI and energy balance-based PET estimates such as, for example, with Penman-Monteith to better accommodate different tropical land use classes and vegetation water use for more detailed biogeochemical simulations of the critical zone. Incorporation of dynamic leaf cycles may dramatically change timing and the integrated magnitude of plant water use, particularly between natural vegetation and crops. Given the potential importance of moisture recycling in the soil-plant-atmosphere continuum at various scales, future research should also consider direct coupling of an isotope-enabled regional climate model to an ecohydrology model with flux tracking for nonstationary water age estimates. Such an approach would provide a basis for projecting future climate and vegetation changes and the impact on the regional hydrological and biogeochemical cycle beyond data scarce tropical catchments.

ACKNOWLEDGEMENTS

We thank the Leverhulme Trust funded ISOLAND (RPG-2018-375) project, the IAEA-CRP F31005 contract 22904, the IAEA-CRP F31006, and the IAEA-CRP F31006 and UCR C1038 funded the IsoRSM project. We also acknowledge the many suggestions by two anonymous reviewers that improved this paper.

DATA AVAILABILITY STATEMENT

The data that support the findings of this study are available from the corresponding author upon reasonable request.

ORCID

Saul Arciniega-Esparza https://orcid.org/0000-0002-1064-5692 Christian Birkel https://orcid.org/0000-0002-6792-852X Ricardo Sánchez-Murillo Dhttps://orcid.org/0000-0001-8721-8093 Dörthe Tetzlaff https://orcid.org/0000-0002-7183-8674 Chris Soulsby https://orcid.org/0000-0001-6910-2118

REFERENCES

Amador, J. A. (2008). The intra-Americas seas low-level jet (IALLJ): Overview and future research. Annals of the New York Academy of Sciences, 1146(1), 153-188. https://doi.org/10.1196/annals.1446.012

Aparecido, L. M. T., Miller, G. R., Cahill, A. T., & Moore, G. W. (2016). Comparison of tree transpiration under wet and dry canopy conditions in a costa Rican premontane tropical forest. Hydrological Processes, 30(26), 5000-5011. https://doi.org/10.1002/hyp.10960

Arciniega-Esparza, S., Birkel, C., Chavarría-Palma, A., Arheimer, B., & Breña-Naranjo, J. A. (2022). Remote sensing-aided rainfall-runoff modeling in the tropics of Costa Rica. Hydrology and Earth System Sciences, 26(4), 975-999. https://doi.org/10.5194/hess-26-975-2022

Bashford, K. E., Beven, K., & Young, P. (2002). Observational data and scale-dependent parameterizations: Explorations using a virtual ARCINIEGA-ESPARZA ET AL. WILEY 19 of 20

- hydrological reality. *Hydrological Processes*, 16, 293–312. https://doi.org/10.1002/hyp.339
- Beven, K. (1995). Linking parameters across scales: Subgrid parameterizations and scale dependent hydrological models. *Hydrological Processes*, 9, 507–525. https://doi.org/10.1002/hyp.3360090504
- Beven, K. J., & Kirkby, M. J. (1979). A physically based, variable contributing area model of basin hydrology/un modèle à base physique de zone d'appel variable de l'hydrologie du bassin versant. Hydrological Sciences Bulletin, 24(1), 43-69. https://doi.org/10.1080/02626667909491834
- Beyer, M., Kühnhammer, K., & Dubbert, M. (2020). In situ measurements of soil and plant water isotopes: A review of approaches, practical considerations and a vision for the future. *Hydrology and Earth System Sciences*, 24, 4413–4440. https://doi.org/10.5194/hess-24-4413-2020
- Birkel, C., Correa Barahona, A., Duvert, C., Granados Bolaños, S., Chavarría-Palma, A., Durán-Quesada, A. M., Sánchez-Murillo, R., & Biester, H. (2021). End member and Bayesian mixing models consistently indicate near-surface flowpath dominance in a pristine humid tropical rainforest. *Hydrological Processes*, 35(4), 1–15, e14153. https://doi.org/10.1002/hyp.14153
- Birkel, C., Correa-Barahona, A., Martinez-Martinez, M., Granados-Bolaños, S., Venegas-Cordero, N., Gutiérrez-García, K., Blanco-Ramírez, S., Quesada-Mora, R., Solano-Rivera, V., Mussio-Mora, J., Chavarría-Palma, A., Vargas-Arias, K., Moore, G. W., Durán-Quesada, A. M., Vasquez-Morera, J., Soulsby, C., Tetzlaff, D., Espinoza-Cisneros, E., & Sánchez-Murillo, R. (2020). Headwaters drive streamflow and lowland tracer export in a large-scale humid tropical catchment. Hydrological Processes, 34(18), 3824–3841. https://doi.org/10.1002/hyp.13841
- Birkel, C., Geris, J., Molina, M. J., Mendez, C., Arce, R., Dick, J., Tetzlaff, D., & Soulsby, C. (2016). Hydroclimatic controls on non-stationary stream water ages in humid tropical catchments. *Journal of Hydrology*, 542, 231–240. https://doi.org/10.1016/j.jhydrol.2016.09.006
- Birkel, C., & Soulsby, C. (2015). Advancing tracer-aided rainfall-runoff modelling: A review of progress, problems and unrealised potential. *Hydrological Processes*, 29, 5227–5240. https://doi.org/10.1002/hyp. 10594
- Birkel, C., Soulsby, C., & Tetzlaff, D. (2014). Developing a consistent process-based conceptualization of catchment functioning using measurements of internal state variables. Water Resources Research, 50(4), 3481–3501. https://doi.org/10.1002/2013WR014925
- Coenders-Gerrits, A. M. J., van der Ent, R. J., Bogaard, T. A., Wang-Erlandsson, L., Hrachowitz, M., & Savenije, H. H. G. (2014). Uncertainties in transpiration estimates. *Nature*, 506(7487), E1–E2. https://doi.org/10.1038/nature12925
- Correa, A., Birkel, C., Gutierrez, J., Dehaspe, J., Durán-Quesada, A. M., Soulsby, C., & Sánchez-Murillo, R. (2020). Modelling non-stationary water ages in a tropical rainforest: A preliminary spatially distributed assessment. *Hydrological Processes*, 34(25), 4776–4793. https://doi. org/10.1002/hyp.13925
- Dehaspe, J., Birkel, C., Tetzlaff, D., Sánchez-Murillo, R., Durán-Quesada, A. M., & Soulsby, C. (2018). Spatially distributed tracer-aided modelling to explore water and isotope transport, storage and mixing in a pristine, humid tropical catchment. *Hydrological Processes*, 32(21), 3206–3224. https://doi.org/10.1002/hyp.13258
- Delavau, C. J., Stadnyk, T., & Holmes, T. (2017). Examining the impacts of precipitation isotope input (\$δ^{18}\$O\$_\mathrm{ppt}\$) on distributed, tracer-aided hydrological modelling. *Hydrology and Earth System Sciences*, 21(5), 2595–2614. https://doi.org/10.5194/hess-21-2595-2017
- Durán-Quesada, A. M., Gimeno, L., & Amador, J. (2017). Role of moisture transport for central American precipitation. *Earth System Dynamics*, 8(1), 147–161. https://doi.org/10.5194/esd-8-147-2017
- Durán-Quesada, A. M., Sorí, R., Ordoñez, P., & Gimeno, L. (2020). Climate perspectives in the intra-Americas seas. Atmosphere, 11(9), 1-32. https://doi.org/10.3390/atmos11090959
- Funk, C., Peterson, P., Landsfeld, M., Pedreros, D., Verdin, J., Shukla, S., Husak, G., Rowland, J., Harrison, L., Hoell, A., & Michaelsen, J. (2015).

- The climate hazards infrared precipitation with stations—A new environmental record for monitoring extremes. *Scientific Data*, *2*(1), 150066. https://doi.org/10.1038/sdata.2015.66
- Giorgi, F. (2006). Climate change hot-spots. *Geophysical Research Letters*, 33, L08707. https://doi.org/10.1029/2006GL025734
- Gleeson, T., & Paszkowski, D. (2014). Perceptions of scale in hydrology: What do you mean by regional scale? *Hydrological Sciences Journal*, 59(1), 99–107.
- Gonfiantini, R., Wassenaar, L. I., Araguas-Araguas, L., & Aggarwal, P. K. (2018). A unified Craig-Gordon isotope model of stable hydrogen and oxygen isotope fractionation during fresh or saltwater evaporation. *Geochimica et Cosmochimica Acta*, 235, 224–236. https://doi.org/10.1016/j.gca.2018.05.020
- González, J. E., Georgescu, M., Lemos, M. C., Hosannah, M. C., & Niyogi, D. (2017). Climate change's pulse is in Central America and the Caribbean Eos. *Transactions of the American Geophysical Union*, 98, 261–268.
- Hastenrath, S., & Polzin, D. (2013). Climatic variations in Central America and the Caribbean. *International Journal of Climatology*, 33, 1348– 1356. https://doi.org/10.1002/joc.3515
- Iraheta, A., Birkel, C., Benegas, L., Rios, N., Sánchez-Murillo, R., & Beyer, M. (2021). A preliminary isotope-based evapotranspiration partitioning approach for tropical Costa Rica. *Ecohydrology*, 2021, e2297. https://doi.org/10.1002/eco.2297
- Jasechko, S., Kirchner, J. W., Welker, J. M., & McDonnell, J. J. (2016). Substantial proportion of global streamflow less than three months old. Nature Geoscience, 9(2), 126–129. https://doi.org/10.1038/ngeo2636
- Jasechko, S., Sharp, Z., Gibson, J. J., Birks, S. J., Yi, Y., & Fawcett, P. J. (2013). Terrestrial water fluxes dominated by transpiration. *Nature*, 496, 347–350.
- Jasechko, S., & Taylor, R. G. (2015). Intensive rainfall recharges tropical groundwaters. Environmental Research Letters, 10(12), 1–7. https://doi. org/10.1088/1748-9326/10/12/124015
- Knighton, J., Saia, S. M., Morris, C. K., Archiblad, J. A., & Walter, M. T. (2017). Ecohydrologic considerations for modeling of stable water isotopes in a small intermittent watershed. *Hydrological Processes*, 31(13), 2438–2452.
- Kühnhammer, K., Dahlmann, A., Iraheta, A., Iraheta, A., Gerchow, M., Birkel, C., Marshall, J. D., & Beyer, M. (2022). Continuous in situ measurements of water stable isotopes in soils, tree trunk and root xylem: Field approval. *Rapid Communications in Mass Spectrometry*, *36*(5), e9232. https://doi.org/10.1002/rcm.9232
- Kuppel, S., Tetzlaff, D., Maneta, M. P., & Soulsby, C. (2018). EcH2O-iso 1.0: Water isotopes and age tracking in a process-based, distributed ecohydrological model. *Geoscientific Model Development*, 11, 3045– 3069. https://doi.org/10.5194/gmd-11-3045-2018
- Landgraf, J., Tetzlaff, D., Dubbert, M., Dubbert, D., Smith, A., & Soulsby, C. (2022). Xylem water in riparian willow trees (*Salix alba*) reveals shallow sources of root water uptake by in situ monitoring of stable water isotopes. *Hydrology and Earth System Sciences*, 26, 2073–2092. https://doi.org/10.5194/hess-26-2073-2022
- Lawrence, D., & Vandecar, K. (2014). Effects of tropical deforestation on climate and agriculture. *Nature Climate Change*, 5, 27–36. https://doi. org/10.1038/nclimate2430
- Lindström, G., Pers, C., Rosberg, J., Strömqvist, J., & Berit, A. (2010). Development and testing of the HYPE (hydrological predictions for the environment) water quality model for different spatial scales. *Hydrology Research*, 4(41.3), 295–319. https://doi.org/10.2166/nh.2010.007
- Mayer-Anhalt, L., Birkel, C., Sánchez-Murillo, R., & Schulz, S. (2022). Tracer-aided modelling reveals quick runoff generation and young streamflow ages in a tropical rainforest catchment. *Hydrological Processes*, 36(2), e14508. https://doi.org/10.1002/hyp.14508
- Min-Venditti, A., Moore, G. W., & Fleischman, F. (2017). What policies improve forest cover? A systematic review of research from Mesoamerica. Global Environmental Change, 47, 21–27. https://doi.org/10. 1016/j.gloenvcha.2017.08.010

- Moore, G. W., Orozco, G., Aparecido, L. M. T., & Miller, G. R. (2018). Upscaling transpiration in diverse forests: Insights from a tropical premontane site. *Ecohydrology*, 11(3), e1920. https://doi.org/10.1002/eco.1920
- Moreira, M. Z., Sternberg, L. A. M., Cictoria, R. L., Barbosa, E. M., Bonates, L. C. M., & Nepstad, D. C. (1997). Contribution of transpiration to forest ambient vapor based on isotopic measurements. *Global Change Biology*, 3, 439–450.
- Mueller, B., & Seneviratne, S. I. (2014). Systematic land climate and evapotranspiration biases in CMIP5 simulations. Geophysical Research Letters, 41, 128–134. https://doi.org/10.1002/2013GL058055
- Muñoz-Jiménez, R., Giraldo-Osorio, J. D., Brenes-Torres, A., Avendaño-Flores, I., Nauditt, A., Hidalgo-León, H. G., & Birkel C. (2019). Spatial and temporal patterns, trends and teleconnection of cumulative rainfall deficits across Central America. *International Journal of Climatology*, 39(4), 1940–1953. https://doi.org/10.1002/joc.5925
- Myneni, R., Knyazikhin, Y., & Park, T. (2015). MOD15A2H MODIS/Terra leaf area index/FPAR 8-day L4 global 500m SIN grid V006 [data set]. NASA EOSDIS land processes DAAC. Retrieved from June 14, 2022 from https://doi.org/10.5067/MODIS/MOD15A2H.006
- Pascale, S., Kapnick, S. B., Delworth, T. L., Hidalgo, H. G., & Cooke, W. F. (2021). Natural variability vs forced signal in the 2015–2019 central American drought. *Climatic Change*, 168(3), 16. https://doi.org/10.1007/s10584-021-03228-4
- Remondi, F., Kirchner, J. W., Burlando, P., & Fatichi, S. (2018). Water flux tracking with a distributed hydrological model to quantify controls on the spatio-temporal variability of transit time distributions. Water Resources Research, 54(4), 3081–3099.
- Reusser, D. E., Buytaert, W., & Zehe, E. (2011). Temporal dynamics of model parameter sensitivity for computationally expensive models with the Fourier amplitude sensitivity test. Water Resources Research, 4(7), 1–14. https://doi.org/10.1029/2010WR009947
- Rodriguez, N. B., & Klaus, J. (2019). Catchment travel times from composite storage selection functions representing the superposition of streamflow generation processes. Water Resources Research, 55(11), 9292–9314.
- Sánchez-Murillo, R., & Birkel, C. (2016). Groundwater recharge mechanisms inferred from isoscapes in a complex tropical mountainous region. Geophysical Research Letters, 43(10), 5060–5069. https://doi.org/10.1002/2016GL068888
- Sánchez-Murillo, R., Durán-Quesada, A. M., Esquivel-Hernández, G., Rojas-Cantillano, D., Birkel, C., Welsh, K., Sánchez-Llull, M., Alonso-Hernández, C. M., Tetzlaff, D., Soulsby, C., Boll, J., Kurita, N., & Cobb, K. M. (2019). Deciphering key processes controlling rainfall isotopic variability during extreme tropical cyclones. *Nature Communica*tions, 10(1), 4321. https://doi.org/10.1038/s41467-019-12062-3
- Sánchez-Murillo, R., Esquivel-Hernández, G., Corrales-Salazar, J. L., Castro-Chacón, L., Durán-Quesada, A. M., Guerrero-Hernández, M., Delgado, V., Barberena, J., Montenegro-Rayo, K., Calderón, H., Chevez, C., Peña-Paz, T., García-Santos, S., Ortiz-Roque, P., Alvarado-Callejas, Y., Benegas, L., Hernández-Antonio, A., Matamoros-Ortega, M., Ortega, L., & Terzer-Wassmuth, S. (2020). Tracer hydrology of the data-scarce and heterogeneous central American isthmus. *Hydrological Processes*, 34(11), 2660–2675. https://doi.org/10.1002/hyp.13758
- Seibert, J., & Vis, M. J. P. (2012). Teaching hydrological modeling with a user-friendly catchment-runoff-model software package. *Hydrology* and Earth System Sciences, 16(9), 3315–3325. https://doi.org/10. 5194/hess-16-3315-2012
- Smith, A., Tetzlaff, D., Kleine, L., Maneta, M., & Soulsby, C. (2021). Quantifying the effects of land use and model scale on water partitioning and water ages using tracer-aided ecohydrological models. *Hydrology and Earth Systems Science*, 25, 2239–2259. https://doi.org/10.5194/hess-25-2239-2021
- Solano-Rivera, V., Geris, J., Granados-Bolaños, S., Brenes-Cambronero, L., Artavia-Rodríguez, G., Sánchez-Murillo, R., & Birkel, C. (2019). Exploring extreme rainfall impacts on flow and turbidity dynamics in a steep,

- pristine and tropical volcanic catchment. *Catena*, 182, 104118. https://doi.org/10.1016/j.catena.2019.104118
- Stadnyk, T. A., & Holmes, T. (2020). On the value of isotope-enabled hydrologic model calibration. *Hydrological Sciences Journal*, 65(9), 1525–1538. https://doi.org/10.1080/02626667.2020.1751847
- Taylor, M. A., Enfield, D. B., & Chen, A. A. (2002). Influence of the tropical Atlantic versus the tropical Pacific on Caribbean rainfall. *Journal of Geophysical Research*, 107, 3127. https://doi.org/10.1029/2001JC001097
- Tian, Y., Woodcock, C. E., Wang, Y., Privette, J. L., Shabanov, N. V., Zhou, L., Zhang, Y., Buermann, W., Dong, J., & Veikkanen, B. (2002). Multiscale analysis and validation of the MODIS LAI product. *Remote Sensing of Envi*ronment, 83(3), 414–430. https://digitalcommons.unl.edu/nasapub/40
- van Huijgevoort, M. H. J., Tetzlaff, D., Sutanudjaja, E. H., & Soulsby, C. (2016). Using high resolution tracer data to constrain water storage, flux and age estimates in a spatially distributed rainfall-runoff model. Hydrological Processes, 30(25), 4761–4778. https://doi.org/10.1002/hyp.10902
- Wei, Z., Yoshimura, K., Okazaki, A., Ono, K., Kim, W., Yokoi, M., & Lai, C. T. (2016). Understanding the variability of water isotopologues in near-surface atmospheric moisture over a humid subtropical rice paddy in Tsukuba, Japan. *Journal of Hydrology*, 533, 91–102. https://doi.org/10.1016/j.jhydrol.2015.11.044
- Welsh, K., & Sánchez-Murillo, R. (2020). Rainfall, groundwater, and surface water isotope data from extreme tropical cyclones (2016-2019) within the Caribbean Sea and Atlantic Ocean basins. *Data in Brief*, 30, 105633. https://doi.org/10.1016/j.dib.2020.105633
- Wohl, E., Barros, A., Brunsell, N., Chappell, N. A., Coe, M., Giambelluca, T., Goldsmith, S., Harmon, R., Hendrickx, J. M. H., Juvik, J., McDonnell, J., & Ogden, F. (2012). The hydrology of the humid tropics. *Nature Climate Change*, 2(9), 655–662. https://doi.org/10.1038/nclimate1556
- Wörner, V., Kreye, P., & Meon, G. (2019). Effects of bias-correcting climate model data on the projection of future changes in high flows. *Hydrology*, 6(2), 1–17. https://doi.org/10.3390/hydrology6020046
- Xiao, W., Wei, Z., & Wen, X. (2018). Evapotranspiration partitioning at the ecosystem scale using the stable isotope method—A review. *Agricultural and Forest Meteorology*, 263, 346–361. https://doi.org/10.1016/j.agrformet.2018.09.005
- Yoshimura, K. (2015). Stable water isotopes in climatology, meteorology, and hydrology: A review. *Journal of the Meteorological Society of Japan. Series. II*, 93, 513–533. https://doi.org/10.2151/jmsj.2015-036
- Yoshimura, K., Kanamitsu, M., & Dettinger, M. (2010). Regional downscaling for stable water isotopes: A case study of an atmospheric river event. *Journal of Geophysical Research*, 115, D18114. https://doi.org/10.1029/2010JD014032
- Yoshimura, K., Kanamitsu, M., Noone, D., & Oki, T. (2008). Historical isotope simulation using Reanalysis atmospheric data. *Journal of Geophysical Research Atmospheres*, 113(19), 1–15, https://doi.org/10.1029/2008JD010074

SUPPORTING INFORMATION

Additional supporting information can be found online in the Supporting Information section at the end of this article.

How to cite this article: Arciniega-Esparza, S., Birkel, C., Durán-Quesada, A. M., Sánchez-Murillo, R., Moore, G. W., Maneta, M. P., Boll, J., Negri, L. B., Tetzlaff, D., Yoshimura, K., & Soulsby, C. (2023). Tracer-aided ecohydrological modelling across climate, land cover, and topographical gradients in the tropics. *Hydrological Processes*, *37*(5), e14884. https://doi.org/10.1002/hyp.14884